11 Computed Tomography/Computed Tomography Angiography for Evaluation, Planning, and Surveillance of Complex Endovascular Repair

Terri J. Vrtiska, Thanila A. Macedo, and Gustavo S. Oderich

Introduction

Endovascular aortic repair (EVAR) has become the first treatment option in most patients with thoracic and abdominal aortic aneurysms. EVAR is also used for other indications including acute aortic syndrome (e.g., dissections, penetrating ulcers, intramural hematomas), coarctation, infection, vasculitis, and traumatic aortic injury. In the last decade, indications for EVAR have been extended to patients with aneurysms and dissections involving the aortic arch, thoracoabdominal, and iliac arteries. This has been possible with development of techniques of branch vessel incorporation using fenestrations, branches, and parallel grafts. Computed tomography (CT) and computed tomography angiography (CTA) are essential to plan aortic repair using either open or endovascular techniques. Its utility in planning endovascular procedures relies on the accurate assessment of etiology, extent of disease, involvement of side branches, adequacy of access vessels, and presence of extra-vascular diseases that might affect treatment selection and approach. However, CT/CTA should not simply be ordered with the expectation that an adequate and informative study will appear at the fingertips of the clinician. Imaging studies often require tailoring the examination to a specific indication and establishing pre-existing protocols in collaboration with radiology colleagues. Communication between multiple specialties, including the radiologist performing the study, is critical to properly address specific questions.

The vast majority of current CT scanners use two-dimensional multi-detector elements (MDCT). The term *CAT scan*, coined in the 1980s to denote *Computed Axial Tomography*, coined a linear array of detector element, which has been replaced by the more advanced MDCT scanner technology. The detectors are mounted in a gantry, which is positioned opposite to the x-ray source. The gantry rotates at a predefined speed continuously in the same direction, while the table moves in a continuous linear fashion through the gantry while it is rotating. The images are obtained in a helical manner over the desired anatomy. This portion of the study is termed acquisition phase, and the data obtained in this phase define the ultimate quality of the study.

The acquired data are then reconstructed into a format that is desired for clinical analysis including the width of slice increments impacting the resolution of the CT examination. Pre-established protocols are useful to standardize imaging in clinical practice to fit specific indications. Post-processing of the source images allows production of many types of images including off-axis multi-planar display and volume-rendered reconstructions that provide a means for clinicians to perform complex measurements and analysis. This chapter summarizes the critical aspects of CT imaging for evaluation, planning, and follow-up of complex endovascular repair in patients with aortic aneurysms and dissections.

Imaging Data

CT imaging data are constructed from small square image elements termed pixels, which are identified by a position in the *x*- and *y*-planes as well as a quantitative radio-density (or Hounsfield unit) in the gray scale color spectrum. The

T.J. Vrtiska (✉)
Section of Vascular CT, Department of Diagnostic Radiology, Mayo Clinic, 200 First Street SW, Rochester, MN 55905, USA
e-mail: vrtiska.terri@mayo.edu

T.A. Macedo
Department of Diagnostic Radiology, Mayo Clinic, 200 First Street SW, Rochester, MN 55905, USA
e-mail: Macedo.Thanila@mayo.edu

G.S. Oderich
Division of Vascular and Endovascular Surgery, Mayo Clinic, 200 First Street SW, Rochester, MN 55905, USA
e-mail: oderich.gustavo@mayo.edu

G.S. Oderich (ed.), *Endovascular Aortic Repair*, DOI 10.1007/978-3-319-15192-2_11

Hounsfield unit (HU) scale is bounded on one end by air, which is represented by black (negative numbers), and on the other end by bone, which is represented by white (positive numbers). Water is neutral and defined as 0 HU. Typically, the *x*–*y* resolution of a CT scan is 0.4–0.6 mm in the axial plane. However, when data are obtained in a helical volumetric format using MDCT, each pixel is also extended in the *z*-plane direction, and represented by a volume rather than planer unit. The volume unit is termed *voxel*. Each voxel has an *x*, *y*, and *z* coordinate and a resolution in the *x*–*y* and *z*-plane. When the resolution in the *x*–*y* and *z* planes is equal, the term *isotropic resolution* is used. Post-processing of reconstructed imaging is most accurate when a scan is acquired and reconstructed as close to isotropic resolution as possible.

Vascular imaging requires a technique to visualize blood-filled structures (arteries and veins) typically represented in a HU spectrum of + 30–45 and separate them from adjacent structures with a similar HU spectrum. To create a larger HU gradient between blood and the adjacent structures, administration of iodinated intravenous contrast provides an HU of +130 or greater in the opacified blood vessel. Ultimately, the ability to discriminate between two voxels depends upon the spatial resolution and the gradient between neighboring voxels based on their relative HU. Many examinations can be acquired using multiphase technique including an acquisition before and after the administration of iodinated contrast material. The pre-contrast acquisition provides an accurate assessment of the vessel wall and can be used to differentiate intramural hematomas from inflammation, as well as assessment of calcification patterns. The arterial, or contrast enhanced phase of the study, best depicts the lumen of the vessel and the early opacification of end organs with contrast. A delayed acquisition can be included to demonstrate regions of the vasculature or organ parenchyma enhancement that opacifies more slowly with contrast, such as an aneurysm sac filled by a retrograde endoleak from the lumbar arteries or a parenchymal infarct involving the spleen or kidneys.

Scan Parameters

The quantity and quality of energy that is generated by the x-ray source of the CT scanner is termed the tube voltage and is measured in peak kilo-voltage (kVp). A high kVp penetrates tissues better, but it has the effect of decreasing gradient of HU between voxels. Therefore, an obese patient requires a high kVp simply to provide enough energy to penetrate the thicker tissue but may result in less optimal tissue separation. A lower kVp can be used in thinner patients or in children, and results in a lower radiation exposure and better contrast differences between tissues. The rate of x-ray production delivered by the x-ray tube per second is represented by milliampere/second (mAs). A higher mAs translates into sharper images because more photons are reaching the detector to create the image. However, as the mAs increases, so does the radiation dose. Most often kVp and mAs are linked and dictated by specific protocols (Table 11.1), but modifications can be made to the acquisition parameters if indicated to optimize image quality dependent on the patient size and examination type.

Table 11.1 Abdominal aortic computed tomography angiogram example of acquisition parameters

Scan type	Spiral
Rotation time (s)	0.5
Collimation	64×0.6
Pitch	1.2
Reference kV	120
Quality reference mAs	240
CARE dose 4D	ON
Breath-hold	Inspiration

Other important factors during MDCT studies are the collimation, which allows regulation of the thickness of the x-ray beam and the table speed or how fast a patient moves through the gantry. Table speed, collimation, and the speed that the gantry rotates define the pitch of the helical data that are acquired. If the table quickly advances a patient through a slowly spinning gantry, the scan will be fast, but the *z*-plane resolution will be poor. Alternatively, if the gantry speed is increased or the table speed is decreased, a tighter spiral of data will be obtained, improving the *z*-plane resolution. Similarly, if a thinner collimation is used, finer data cuts are acquired. In general a pitch less than one is optimal for subsequent image reconstructions, but newer MDCT scanners use alternative reconstruction algorithms that do not allow a simple calculation of the pitch.

In some locations such as the aortic valve or ascending aorta, the temporal resolution of scans is important because of the dynamic nature of the vascular beds impacted by hemodynamic forces and pulsatility. Electrocardiography (ECG) gating is a technique that allows the acquisition of data during a specific phase of the cardiac cycle (usually during diastole) or during multiple points during a cardiac cycle. Although technological advancements have minimized the need to slow heart rates during ECG-gated MDCT, it is important that patients are not tachycardic. Irregular heart rate can also make cardiac gating challenging and result in image degradation. These scans often have higher radiation exposure and limited scan length, which reduces its utilization in patients with thoracic and thoracoabdominal aortic disease. Its primary indications are for patients with involvement of the aortic valve, the ascending aorta and aortic arch. Multiphase studies can be acquired that depict data throughout the cardiac cycle (as many as 20 phases) and illustrate four-dimensional anatomy, with change in the cardiac anatomy over time being the fourth dimension. Thus specific

measurements can be made during peak systole and end diastole establishing a range of diameters of the vessel over the cardiac cycle.

Reconstruction

The data acquired from an MDCT scan are reconstructed into two-dimensional axial images with a slice thickness. The thickness of the slices may overlap, so that the same point in three-dimensional (3D) space on the patient is represented on two different slices. This method optimizes the spatial resolution of the study and helps to improve the accuracy of volumetric 3D-reconstruction. Multi-planar reformatting (MPR) is the most common method used to display a CT scan today (Fig. 11.1), and it typically consists of a panel that depicts the axial, coronal, and sagittal reconstructions. However, because the data exist in three dimensions, the angle of each planar reconstruction can be modified, allowing the clinician to interpret the specific relationships among the various structures.

Maximum intensity projections (MIPs) are created by projecting the voxels created up to a maximum value into a visualization plane. The voxels are grouped and projected at a uniform HU value that is equal to the highest HU value within the grouping of points. This connects the high-intensity regions of contrast-enhanced vessels in three dimensions, which can then be viewed from any projection. As vessels that pass back and forth between planes, they can be viewed by scrolling through any one of the imaging sets. Alternatively, a curved MPR can be created that allows interpretation of a specific vascular bed. This is done by creating a reconstruction of the images along the centerline of flow (CLF) of a vessel (Fig. 11.2).

MIP images define the borders of a vessel, allowing the geometric center to be calculated. The dots representing the center of the vessel lumen in 3D space are connected to form the CLF. The vessel can be projected along a curved CLF or a straightened CLF. Although there is some debate into which is the best method to measure vessel diameter, most experts use CLF projections (Fig. 11.3). An image is reconstructed that is perpendicular to the CLF, and the diameter of

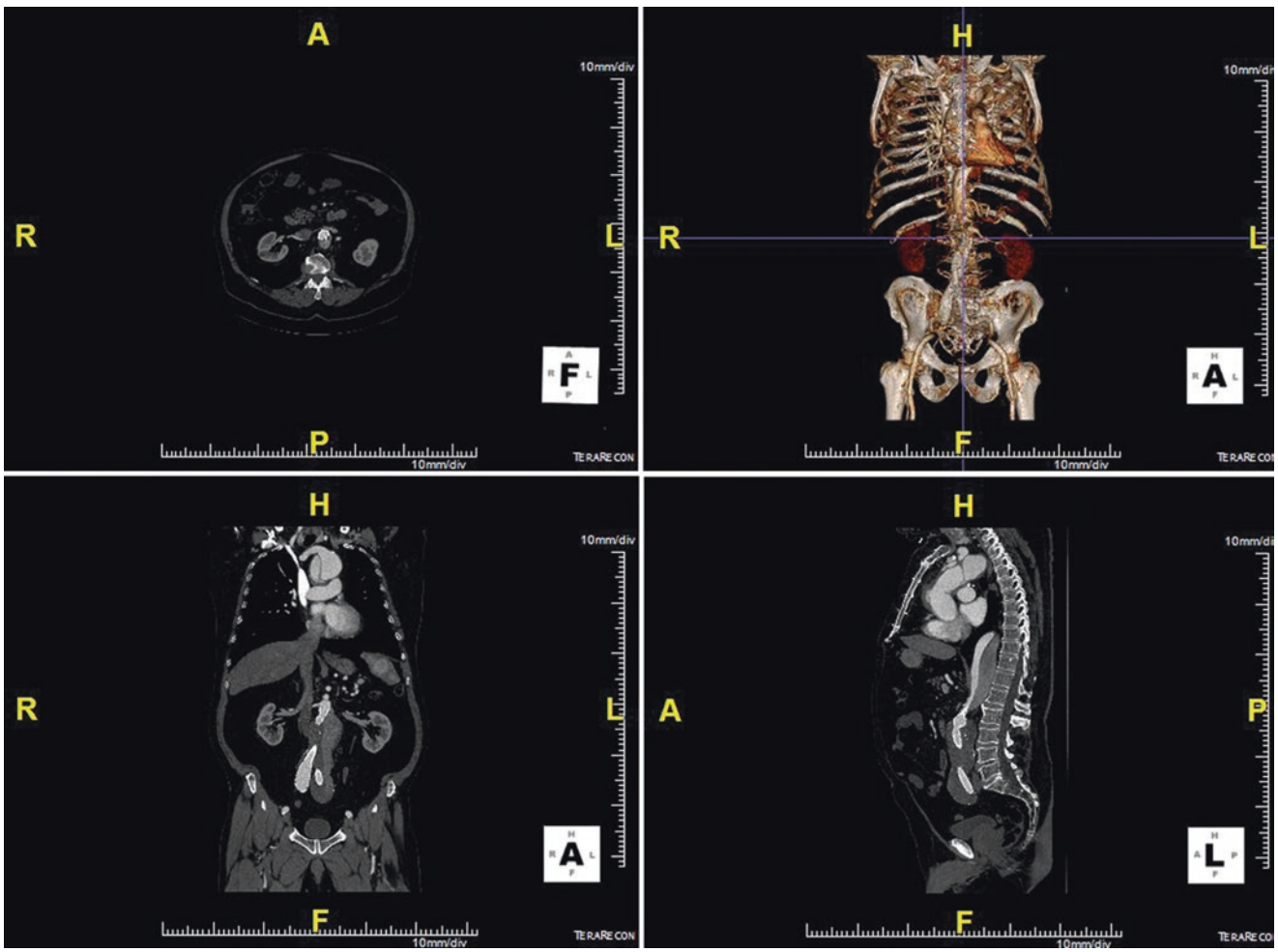

Fig. 11.1 Multi-planar reformatting (MPR) typically includes a panel that depicts the axial, coronal, and sagittal reconstructions. By permission of Mayo Foundation for Medical Education and Research. All rights reserved

Fig. 11.2 The tortuous aorta (**a**) is evaluated using centerline of flow analysis (CLF, **b**). A curved multi-planar reformatting (MPR) image is created to analyze specific segments of the vessel (**c**). The straightened CLF is used for measurements of lengths and to assess the extent of aortic disease (**d**). By permission of Mayo Foundation for Medical Education and Research. All rights reserved

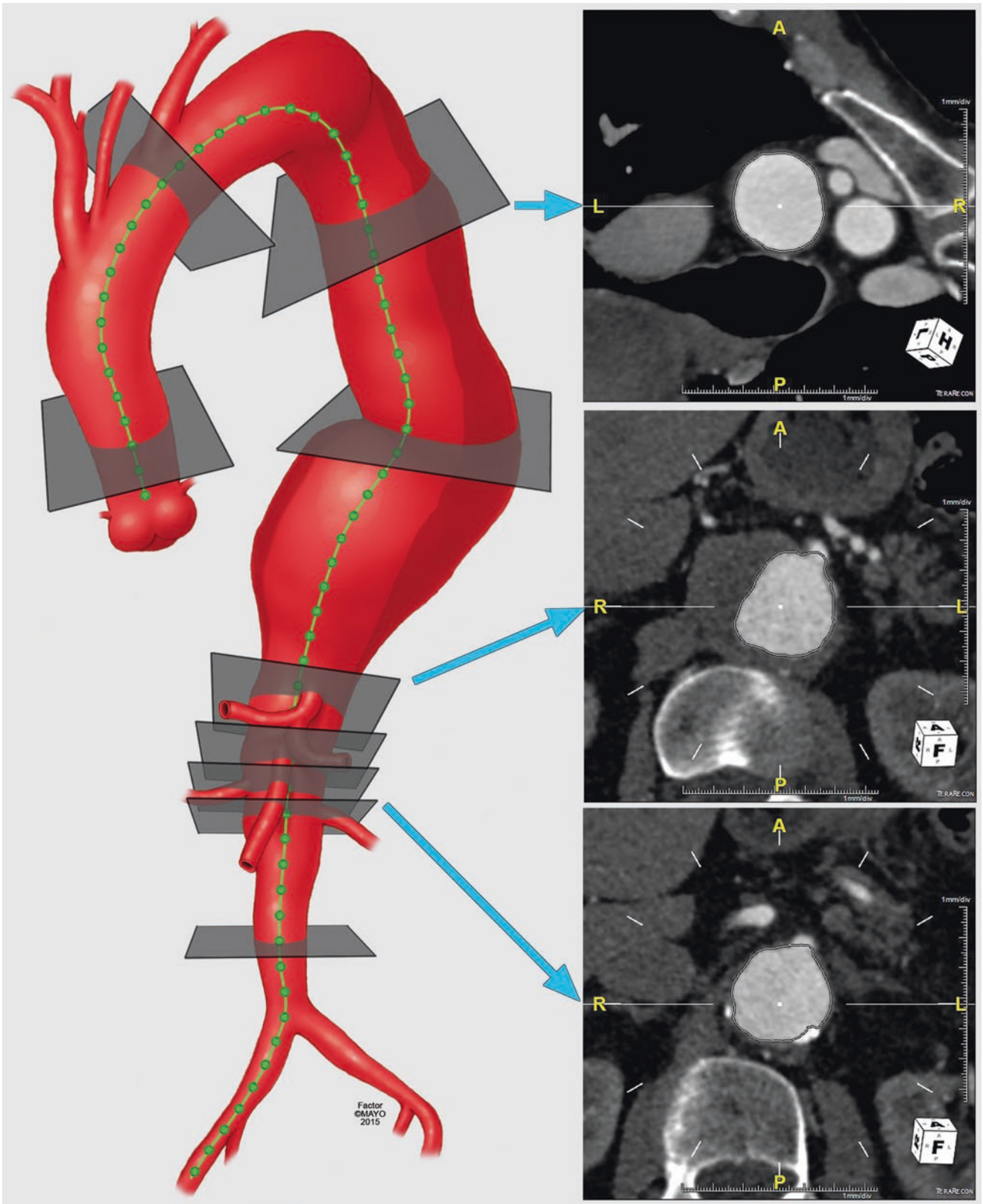

Fig. 11.3 Use of centerline of flow to evaluate aortic diameters in each specific segment. By permission of Mayo Foundation for Medical Education and Research. All rights reserved

Table 11.2 Scanning protocols for abdominopelvic CT and CT angiography (CTA) examinations[a]

	CT		CTA	
Parameter	Routine	Liver or pancreas	Thoracic, abdominal, extremity	Renal artery
Scan type	Spiral	Spiral	Spiral	Spiral
Rotation time (s)	0.5	0.5	0.5	0.5
Collimation (mm)	128×0.6	128×0.6	128×0.6	128×0.6
Pitch	0.8	0.8	0.4 for extremities, 0.6 for others	0.6
Reference tube potential (kV)	120	120	120	120
Quality reference mAs	240	350	250	350
CARE kV	On	On	On	On
CARE kV strength	8	6	11	11
CARE dose 4D	On	On	On	On

[a]Adapted from Yu L, Fletcher JG, Grant KL, Carter RE, Hough DM, Barlow JM, Vrtiska TJ, et al. Automatic selection of tube potential for radiation dose reduction in vascular and contrast-enhanced abdominopelvic CT. AJR Am J Roentgenol. 2013 August; 201 (2): 297–306
Reprinted with permission from the American Journal of Roentgenology

the vessel is measured from this image. This obviates the need to obtain the maximum/minimum diameters of vessels from images that may cut obliquely through a vessel, which create an inconsistent and less accurate way to measure the diameter of aneurysms or stenosis.

Standardized Protocols

CT angiogram acquisitions are adapted according to the clinical question as well as potential interventions. Typically the examinations are performed on state-of-the-art scanner technology (128-MDCT scanners or greater) in order to provide the optimal image resolution at the lowest radiation dose. The examinations are acquired with a spiral technique and a rotation time of 0.5 s. A typical detector configuration is 128×0.6 mm with a pitch of <1. Traditionally, 120 kVp has been used for the average-sized patients, however, using newer technologies such as auto-kV accompanied with technological scanner advances allow the scans to be acquired at a lower kVp without compromising image quality. Automatic exposure control (AEC) is also an advanced technique used in all CT angiogram studies in order to adjust the tube current based on the specific size and shape of the patient resulting in considerable radiation dose reduction (40–60 %) compared to earlier CT acquisitions without AEC. Administration of iodinated intravenous contrast material volume is also adjusted to the patient size typically using 80–140 ml of contrast material although recent scanner advancement allows consistent arterial opacification with volumes as low as 40–50 ml. The rate of contrast injection for an arterial study most commonly is performed at 4–5 ml/s followed by 25 ml of normal saline in order to flush the contrast material from the arm veins and use the full contrast bolus in the CTA acquisition. Examples of standard CT angiogram acquisitions are given in Table 11.2.

Special Protocols

Low Radiation

A regular requirement for CT scanning is optimization of radiation dose to follow the ALARA principle, or As Low As Reasonably Achievable. This requirement is applied to every CTA study but is especially important when considering examinations in young patients, patients undergoing repetitive examinations or multiphase CT acquisitions. Current CT scanners have been optimized to use the radiation dose most efficiently from the electronic components as well as decreasing noise within the CT examinations. Automatic exposure control is now established as a necessary addition to nearly all CT examinations and individualizes the tube current to each patient. Other radiation lowering techniques include Auto kV, which typically lowers the kilovolts for the patient based on the patient size. A simple way to also lower the radiation dose for every examination is to limit the acquisition coverage and number of acquisitions to only those needed for the specific study. For example, only scanning the length of an endovascular stent in follow-up can markedly reduce the radiation dose rather than "over-scanning" the entire chest, abdomen and pelvis, if not clinically indicated. Finally, ongoing advancements in iterative reconstruction (IR) techniques allow CT examinations to be obtained at a lower dose (e.g., greater noise), which are then processed to improve the visualization of vascular and other structures to match examinations that would have been obtained at a higher radiation dose.

Low Contrast

Using lower volumes of iodinated contrast material (renal-sparing protocols) is possible with the latest CT technology (Fig. 11.4). For example, the amount of iodinated contrast

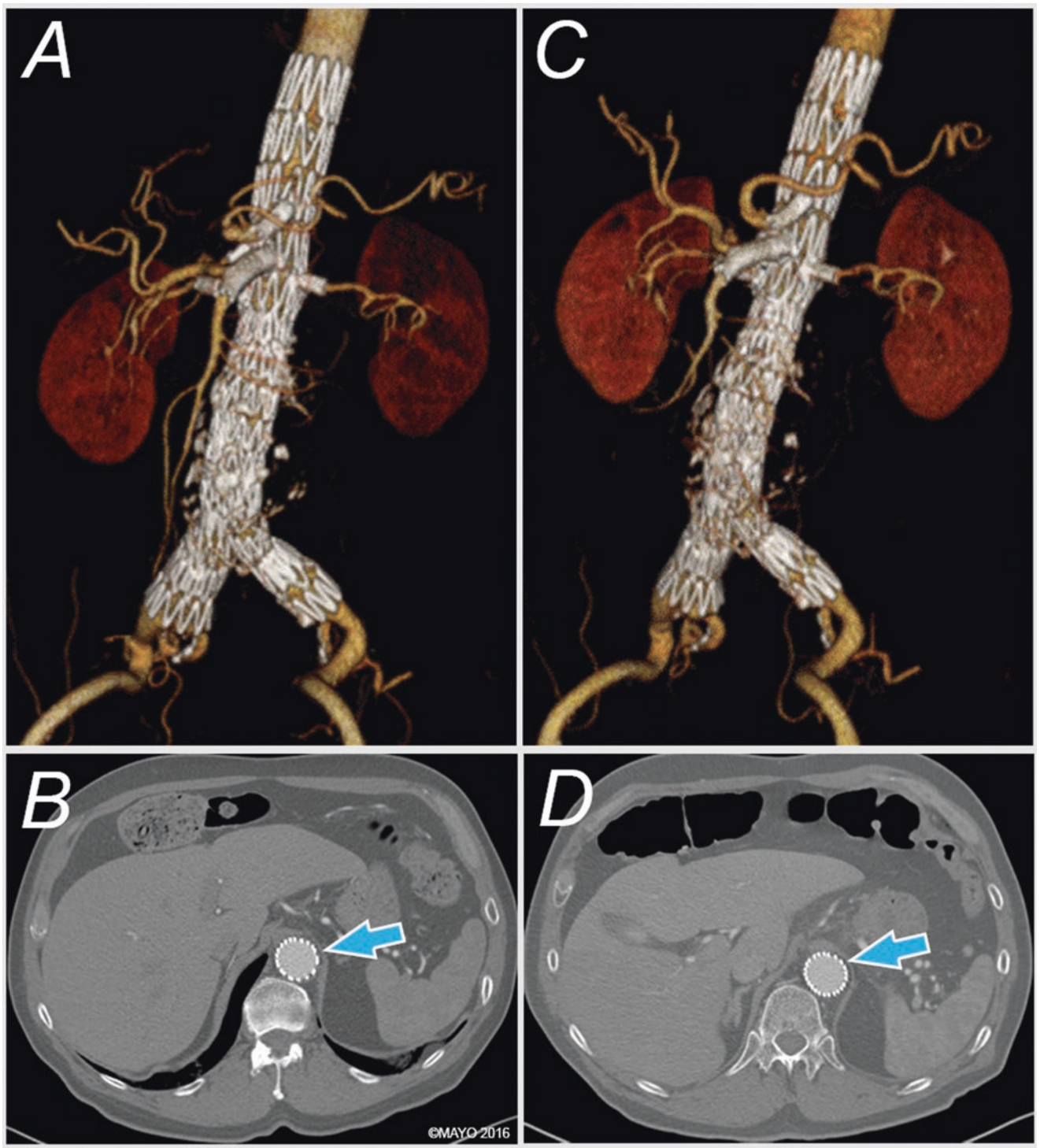

Fig. 11.4 A 74-year-old male with two postoperative CT angiograms. (**a**, **b**) A volume-rendered image and axial CTA acquired on the third-generation dual-source dual-energy CT scanner required only 50 ml of IV contrast material. (**c**, **d**) A traditional CT angiogram obtained 4 months later used a full-contrast bolus of 140 ml of IV contrast. Note that there is no change in the aortic enhancement using the smaller amount of IV contrast (*arrows*). By permission of Mayo Foundation for Medical Education and Research. All rights reserved

material can be markedly reduced in the third-generation dual source CT scanners (SOMATOM FORCE; Siemens Healthcare, Malvern, PA) through improvements in the x-ray tube, which has a smaller focal spot accompanied by a larger x-ray generator. The impact of these changes allows low kV scanning to be performed. There is improved visualization of iodine at lower doses of IV contrast and at a lower kV. Using these newest CT scanners, IV contrast volumes can be reduced to 30 % of prior IV contrast injections (e.g., 50 ml or less), with acceptable image quality and confidence in

diagnostic review. The ability to give the smaller doses of contrast material is especially useful in patients with poor renal function who may undergo multiple catheter interventions as well as multiple CT angiograms for preoperative and postoperative assessment.

Intra-arterial Injection

Approximately one-third of the patients with complex aortic aneurysms have Stage III or greater chronic kidney disease. Contrast-induced nephropathy continues to be a controversial topic, and to generate significant anxiety from patients and physicians. Prior to use of low-contrast CT protocols specified above, we have evaluated intra-arterial contrast injection for CTA to plan endovascular repair with fenestrated and branched endografts in patients with severe renal dysfunction. This was used selectively in a few patients with Stage IIIb or IV chronic kidney disease. The IA-CTA protocol required placement of a 5Fr transfemoral flush catheter, which was positioned in the proximal descending thoracic aorta. IA-CTA was obtained using helical MDCT scanner with total of 40 ml of non-ionic contrast agent diluted in 80 ml of normal saline and injected at 8 ml/s for 15 s (Fig. 11.5). Although the quality of the studies was considered satisfactory to plan the procedures, the need for placement of intra-arterial catheter under fluoroscopy and the added cost represented major limitations. More recently, the availability of third-generation dual source CT scanners (SOMATOM FORCE; Siemens Healthcare, Malvern, PA) and low-contrast protocols eliminated the need for IA-CTA.

Initial Aortic Assessment

All patients with aortic pathology need assessment of the entire aorta using CT, CTA, magnetic resonance imaging (MRI) or magnetic resonance angiography (MRA), irrespective of the disease extent, or whether the primary problem is an aneurysm, dissection, or other aortic disorder (Fig. 11.6). The importance of a thorough imaging evaluation relies on the incidence of concomitant multi-segment disease in 10–25 % of patients, and the need to assess the arch and iliofemoral arteries to evaluate the risk of stroke and anticipate access challenges. A single-phase CTA is typically performed of the chest, abdomen, and pelvis for the initial examination. However, the study can be adapted to include pre-contrast or delayed images depending on the specific indication. If the proximal aorta is not diseased, the subsequent CTAs are tailored to image only the relevant anatomy such as the abdomen and pelvis, and the number of phases and longitudinal extent of the examination is decreased to limit the radiation dose. In patients who have arterial wall thickening identified on CTA, the pre-contrast phase is used to ascertain the presence of blood (hematoma) in the aortic wall rather than inflammation that may be associated with rapid growth or an arteritis. The non-contrast phase also provides an assessment of calcifications.

The aorta and its branches are evaluated for stenosis or dilatation on the optimal phase of arterial enhancement. This should be done in a systematic manner, usually relying upon the axial images. Scrolling through the axial images, the aorta is inspected first, followed by each of the main aortic branches, including the supra-aortic trunks, the celiac, superior mesenteric artery (SMA), renals, and internal iliac arteries. When pathology is noted and specific measurements are needed, one can rely upon MIP images and the creation of CLF for the assessment of luminal narrowing, and the projection of images perpendicular to the CLF for measurements of the outer wall diameter. These data are used to establish a diagnosis and assist with the planning of treatment for patients with aortic disease.

Analysis of Disease Extent

Arteries are cylindrical and have decreasing diameter as they travel distally through the circulation. Disease assessment is performed using surrogates such as changes in diameter or presence of arterial wall abnormalities such as calcium, thrombus, debris, or thickening. The vessel wall, in the absence of any pathology, is difficult to accurately quantify on most CT studies. A vessel wall that appears thick or is lined by atherosclerotic debris indicates pathology and should be further evaluated. Aortic aneurysms are traditionally classified according to which specific segment and side branches they involve. Figures 11.7 and 11.8 summarize proposed nomenclature based on extent of disease by CTA for complex abdominal and thoracoabdominal aortic aneurysms. Aortic disease moves cranially with progressive involvement of side branches. Therefore, it is not infrequent that very large aneurysms have signs of disease affecting the renal and mesenteric arteries, or the aorta in the chest. CTA imaging has revolutionized assessment of extent of aortic disease, which plays a critical role on selection of treatment method or extent of aortic replacement.

CLF studies provide the greatest amount of information when carefully assessing the aorta. The area of aortic dilatation can be readily identified, compared with adjacent segments, and evaluated for specific vessel involvement. When evaluating the results of treatment, the extent of disease and presence of specific complications such as endoleaks, device integrity issues, stenosis, occlusions, migration, or disconnections,

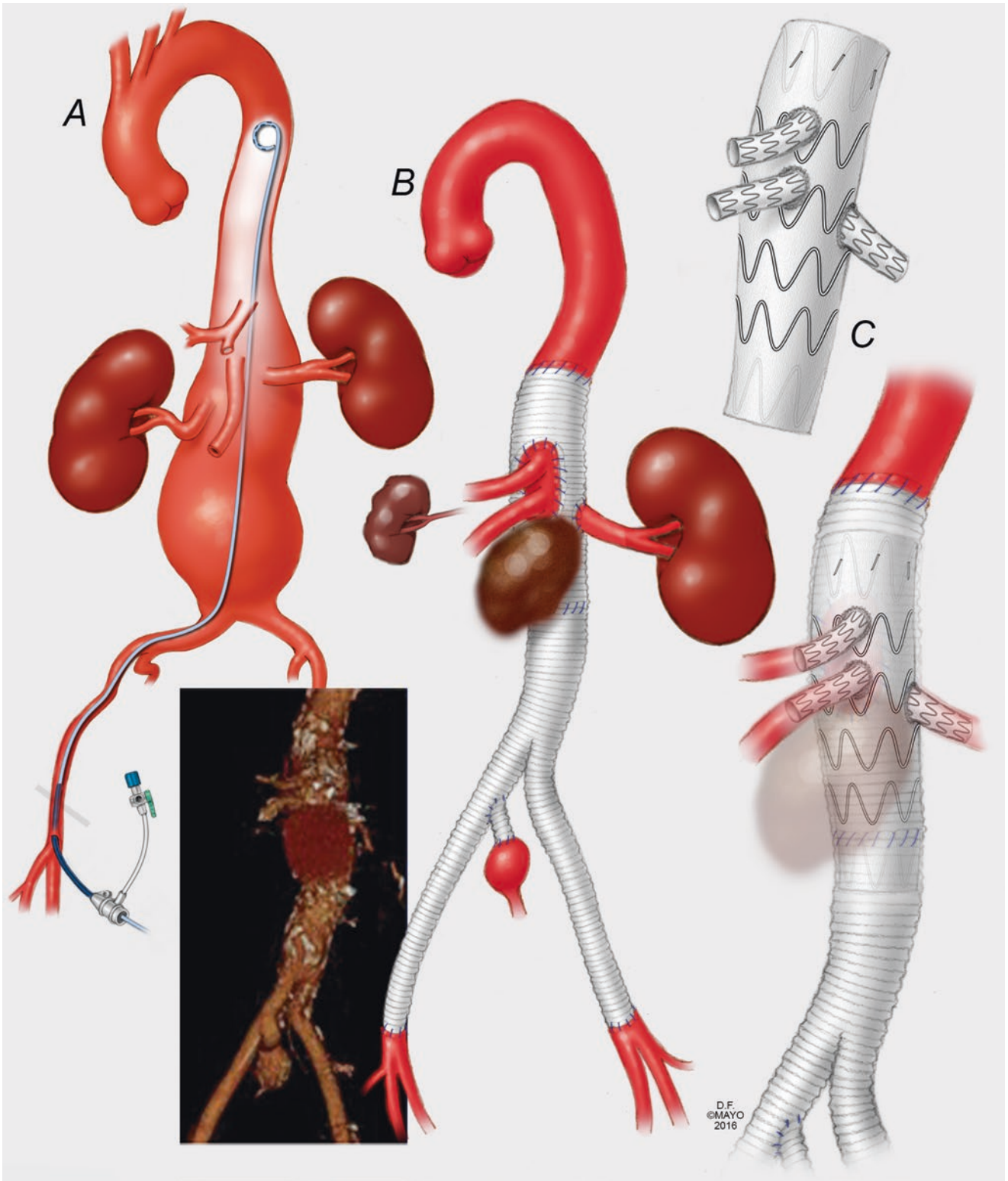

Fig. 11.5 Technique of intra-arterial contrast injection for computed tomography angiography (IA-CTA). Using trans-femoral arterial access, a flush diagnostic catheter with no radiopaque markers is positioned in the proximal thoracic aorta (**a**). In the case presented, a patient with severe renal dysfunction and a large acute pseudo-aneurysm at the level of the mesenteric arteries (**b**) is evaluated by IA-CTA and immediately taken to the hybrid endovascular room for emergency repair using a modified fenestrated graft (**c**). By permission of Mayo Foundation for Medical Education and Research. All rights reserved

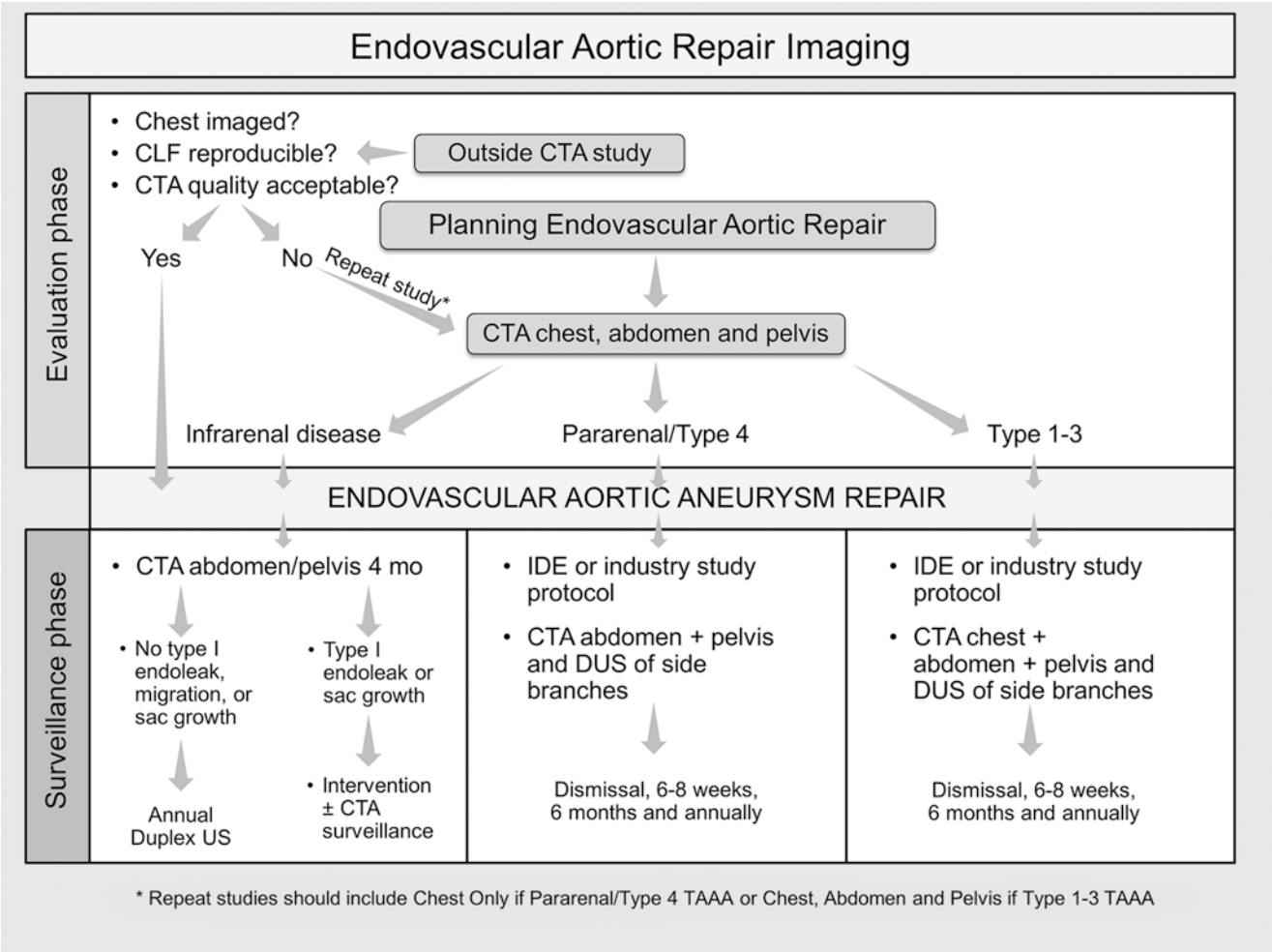

Fig. 11.6 Mayo Clinic protocol of computed tomography angiography evaluation prior to endovascular repair according to extent of aortic disease. By permission of Mayo Foundation for Medical Education and Research. All rights reserved

should be interpreted and categorized in accordance with the published reporting standards of the Society of Vascular Surgery for reports dealing with abdominal aortic aneurysms, thoracic, and thoracoabdominal aortic aneurysms.

Aneurysm Size Measurements

Significant progress has been made since the time where aneurysms were measured using very rudimentary techniques. Early CT scans were used to evaluate the aorta, but vessel tortuosity posed some challenges. Because the aorta is often tortuous in aneurysmal segments, slices from nonhelical CT studies provide an elliptical section of the vessel, which most often represents the obliquity of the plane intersecting with the vessel rather than an unusually shaped aorta. Clinicians generally agree that the minimal diameter of the vessel in a given slice of a CT scan most closely represents the maximal diameter of the aneurysm. Current reconstruction techniques make aneurysm size assessment both simpler and more reproducible, allowing analysis of the aneurysm morphology and selection of optimal location, projection, and technique to measure the largest aneurysm diameter. This requires analysis of imaging in the axial, coronal, sagittal planes as well as CLF (see Fig. 11.3).

In general, diameter measurements should always be made perpendicular to the CLF. This can be done manually using MPR projections, by aligning two of the three planes orthogonal to the measurement plane, or using automated technique and CLF with an orthogonal image projection. CLF measurements of maximum diameter allow any unusual vessel morphology to be accurately depicted on the reconstructed image. Volume calculation can also be obtained and may be a more accurate representation for assessment of aneurysm sac enlargement, given that any maximal aneurysm diameter measurement is representative of a single location. However,

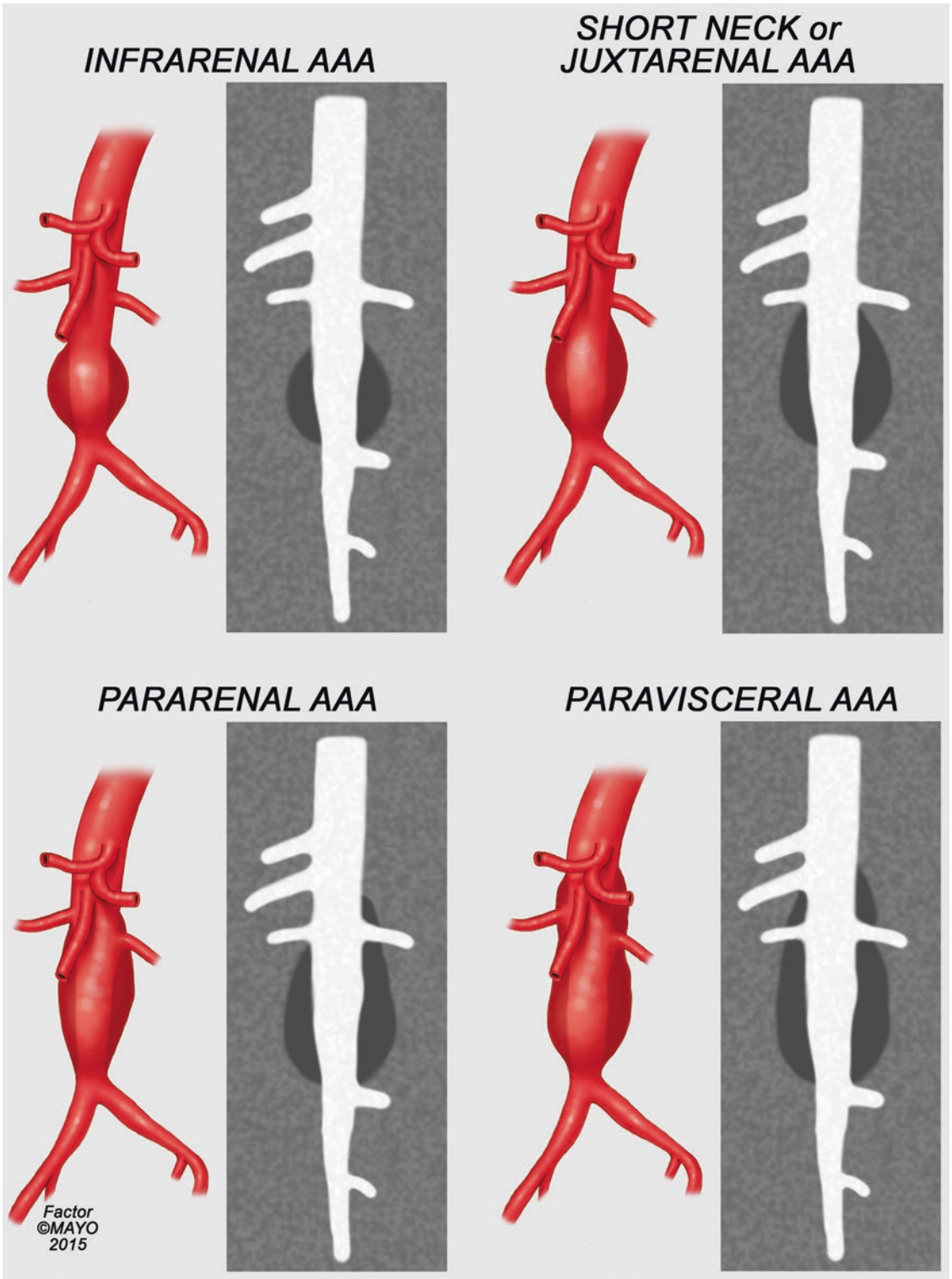

Fig. 11.7 Proposed nomenclature for complex abdominal aortic aneurysms based on analysis of parallel aortic wall by computed tomography angiography. By permission of Mayo Foundation for Medical Education and Research. All rights reserved

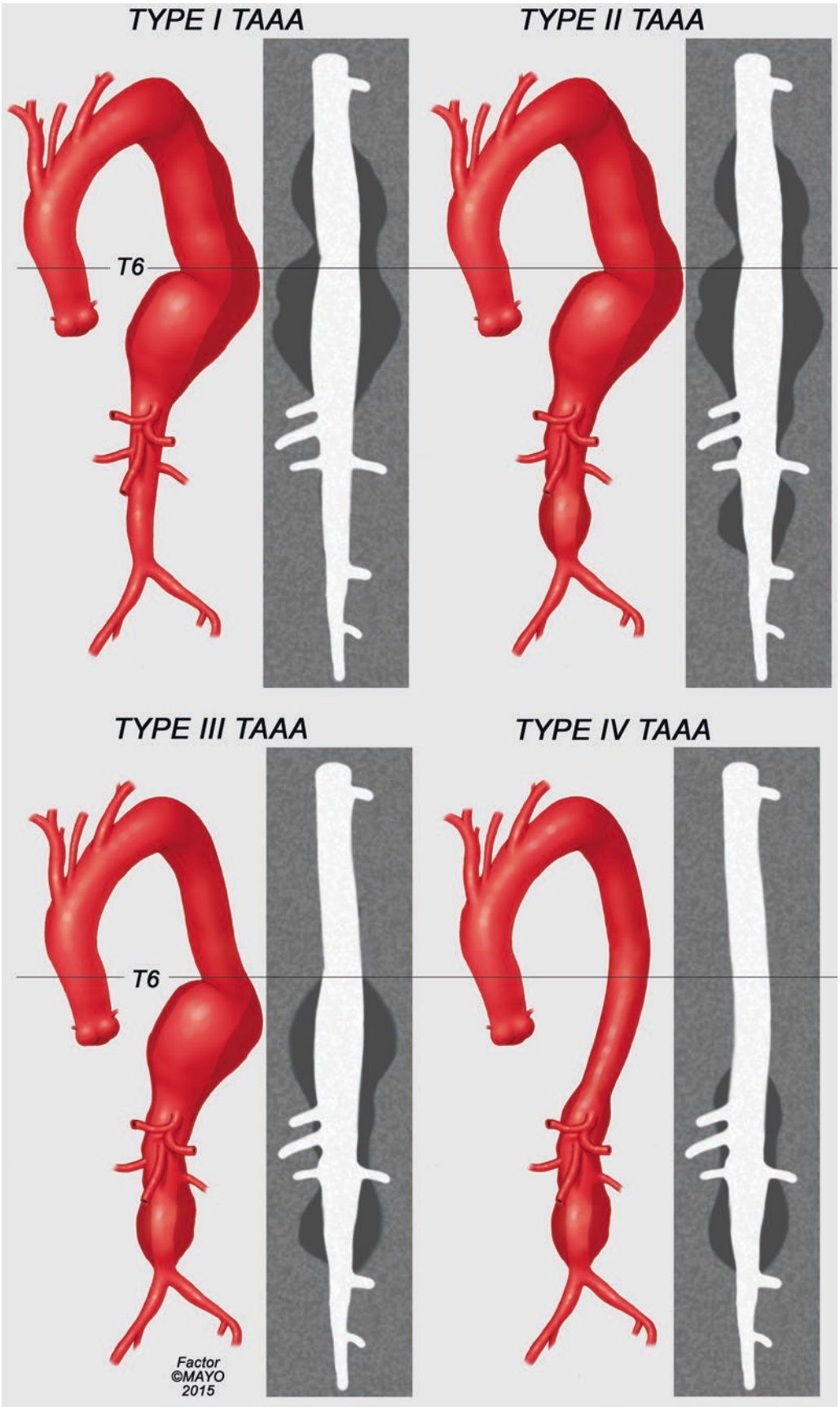

Fig. 11.8 Proposed nomenclature for thoracoabdominal aortic aneurysms based on analysis of parallel aortic wall by computed tomography angiography. By permission of Mayo Foundation for Medical Education and Research. All rights reserved

natural history studies that describe estimates of rupture risk are uniformly based on diameter and not on volume.

Measurement of aneurysm volume is performed with identification of the outer wall of the aneurysm sac. Given that vessel wall, atheroma, adjacent psoas musculature, and inferior vena cava have similar HUs, automated calculations are challenging or practically impossible. Several software programs provide volume measurements. It remains to be determined whether volume is important with regard to the initial assessment of an aneurysm, but few would argue that volume assessment is more sensitive at detecting size changes following treatment of aneurysms with endovascular devices. The necessity of such measurements is questioned, but when they are readily available, they are potentially useful.

Recent reports have also analyzed the effect of specific aneurysm morphology with respect to rupture risk. The use of complex engineering calculations termed *finite element analysis* can determine regions of high wall stress, which may be more prone to rupture. This is often in the posterior lateral wall of the aorta, which correlates clinically with the most common location for aneurysm rupture.

Assessment of Landing Zones

The most important strategic decision on planning any open surgical or endovascular aortic repair is the selection of the proximal and distal anastomotic or landing sites. For open repair, the surgeon identifies areas that are safe for placement of a clamp, and are relatively free of calcification and thrombus, and ideally free of aortic disease. Although the graft can be anastomosed to areas of relative mild aortic enlargement, for endovascular stents a normal segment needs to be selected given that there is continued neck growth after placement of a self-expandable stent (Fig. 11.9). Endovascular repair therefore requires a length of healthy aorta or iliac artery to allow circumferential stent-graft apposition to the vessel wall, creating a seal zone and allowing adequate fixation of the device by active mechanism.

Analysis of neck morphology is one of the most important surrogates in selection of healthy aorta (Fig. 11.10). Areas that have extreme tortuosity or that appear conical, non-cylindrical, and segments that contain atheromatous debris, thrombus or calcification are not considered safe regions to clamp, sew a graft or to fix and seal endovascular devices. Ideally, assessment of landing zones is best done using CLF projections (Fig. 11.11). A segment that is reasonably straight and that appears otherwise healthy and without calcification, thrombus or significant change in diameter (>10 % variation), and that is smaller than adjacent proximal aortic segments, is considered normal aorta for placement of endograft.

Open surgical grafts can be tailored intra-operatively depending on specific anatomy. For endovascular repair, planning needs to be completed pre-operatively to allow selection of all anticipated modular devices. Patient-specific thoracoabdominal devices also tailored to the anatomy with respect to the number and location of fenestrations and branches, changes in stent diameter, and location of sealing zones. Longitudinal distance measurements can be obtained from CLF projections, including the straightened or stretched view, and diameter measurements are obtained from orthogonal projections. Each of the commercially available endografts has identified minimum length and diameter requirements for the proximal and distal landing zones, which are based upon their analysis of the device behavior in vivo and in vitro. This information is available in the instructions for use of each type of device. Additionally, many processing imaging software vendors have specific programs that aid with the planning and sizing of devices.

Tortuosity

Aneurysms grow in diameter and in length, which accounts for varying degrees of tortuosity in certain segments of the aorta. Because the supra-aortic trunks and the renal-mesenteric arteries represent fixating points in the aorta, the most frequent areas of significant tortuosity are in the mid segment of the thoracic aorta and in the infra-renal aorta adjacent to the renal arteries. In general, larger aneurysms tend to be associated with more tortuosity compared to smaller aneurysms. It is difficult to define tortuosity using 3D imaging. Any 3D projection can be reduced to 2D, and the maximal angle can be calculated. Although this technique is what was used to define proximal neck angulation in most studies of AAA endografts, the information is of limited use. Iliac tortuosity is even more difficult to quantify. This is usually done with a scale of mild, moderate, and severe.

The arch represents a special challenge because of its natural curved geometry and the differences in length between the greater and the lesser curvatures of the arch. The location of the supra-aortic trunks can be variable in 25 % of the patients, and arch curvature changes with age.

Branch Assessment

Complex aortic aneurysms by definition involve side branches. The presence of concomitant occlusive or aneurysmal disease of the aortic branches is critical to determine candidacy to fenestrated and branch grafts and the specific design and approach. Minimum requirements are diameters from 4 to 11 mm and absence of early vessel bifurcation (Fig. 11.12). Qualitative assessment can be made from careful inspection of imaging, and when suspicion arises, more detailed imaging processing is helpful. Images perpendicular to the vessel are most helpful, and this can be obtained manually using MPR projections or with CLF. Arterial narrowing, diameter measurements, and

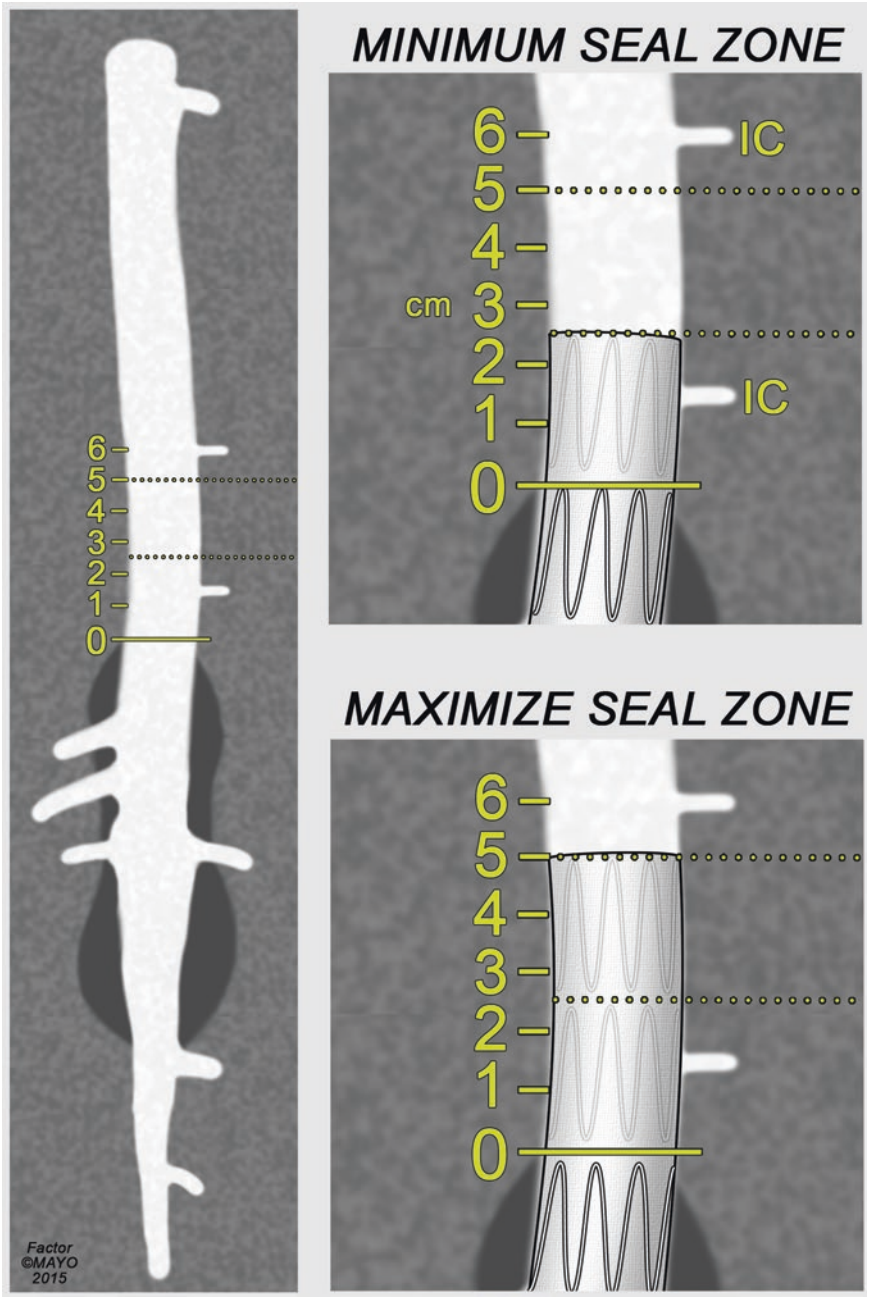

Fig. 11.9 Selection of minimal proximal landing zone based on parallel aortic wall. Note a landing zone of 2.5 cm is selected, but this is extended proximally just below the next intercostal arterial station to maximize seal at the proximal attachment site. By permission of Mayo Foundation for Medical Education and Research. All rights reserved

assessment of branch vessel length before bifurcations can be obtained using these techniques. The same criteria that are applied to determine the quality of the aorta and its sealing zones are used to establish vessel involvement by aneurysm or atherosclerotic disease. A cylindrical vessel with proper distal tapering of diameter and absence of atheromatous debris indicate normal anatomy. Also calcifications can be determined from pre-contrast studies or by using a window leveling technique. Volumetric analysis of the renal parenchyma is done to assess estimate of volume in patients with large accessory renal arteries or early branch bifurcation (Fig. 11.13).

Branch Vessel Geometry

The development of specially designed stents to incorporate aortic side branches has created a need to assess and accurately describe the 3D geometry of the aorta around the renal-mesenteric arteries. Vessel triangulation or the special relationship between the origins of all four visceral arteries allows precise planning of fenestrated and branched endografts. A CLF projection is used and the proximal sealing and fixation section of the aorta is chosen upon the appearance of healthy aortic tissue as previously described. The distance between the center of

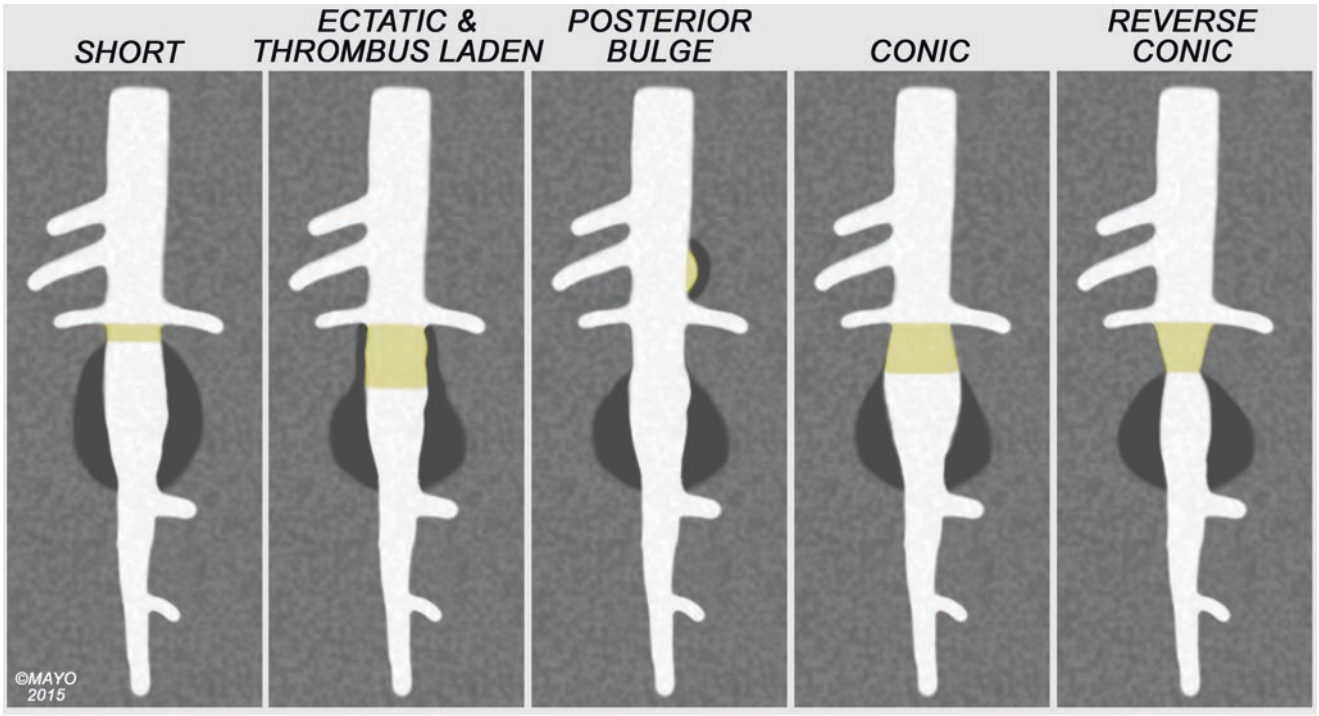

Fig. 11.10 Unsuitable landing zones for endovascular aortic repair include short, ectatic or thrombus laden aorta, posterior bulge, conic or reverse conic necks. By permission of Mayo Foundation for Medical Education and Research. All rights reserved

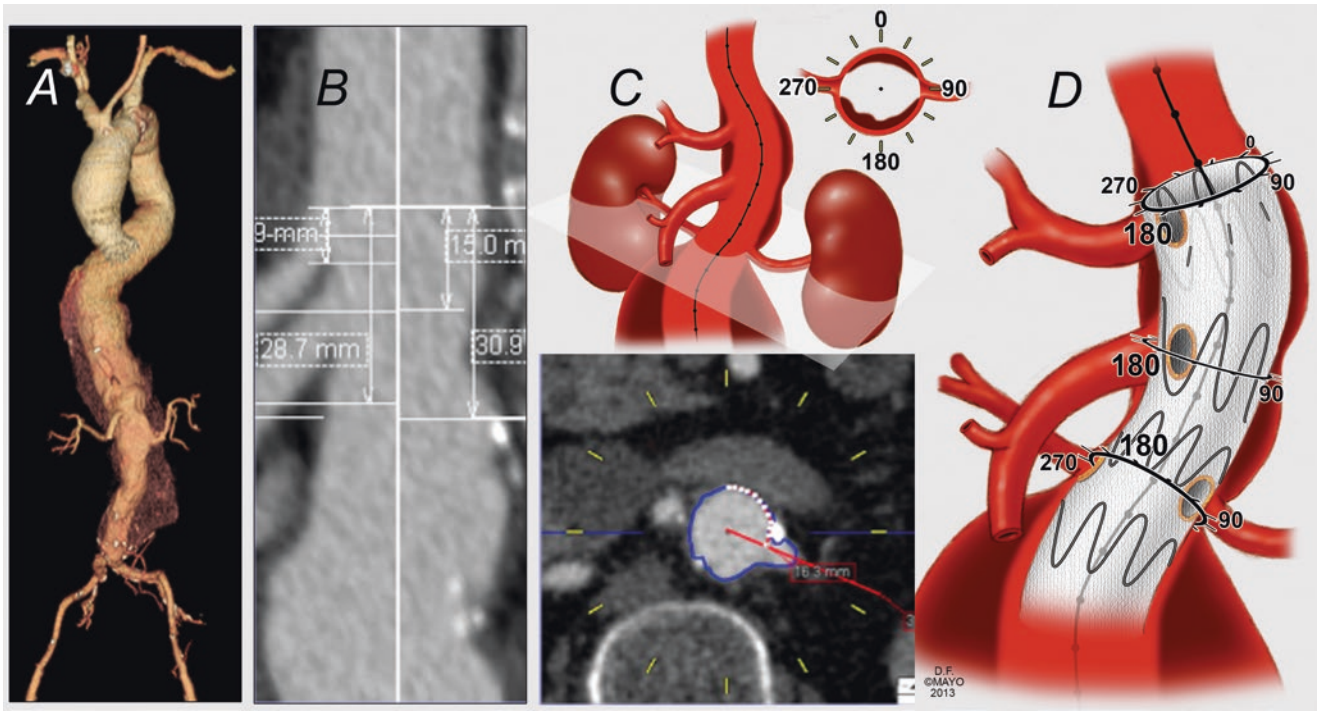

Fig. 11.11 Computed tomography angiography (**a**) is analyzed using centerline of flow (**b**). The proximal landing zone is selected above the celiac axis (**c**). Vessel triangulation technique using length measurements (**b**) coupled with axial clock orientation of each target (**c**) allows precise planning of fenestrated endografts (**d**). By permission of Mayo Foundation for Medical Education and Research. All rights reserved

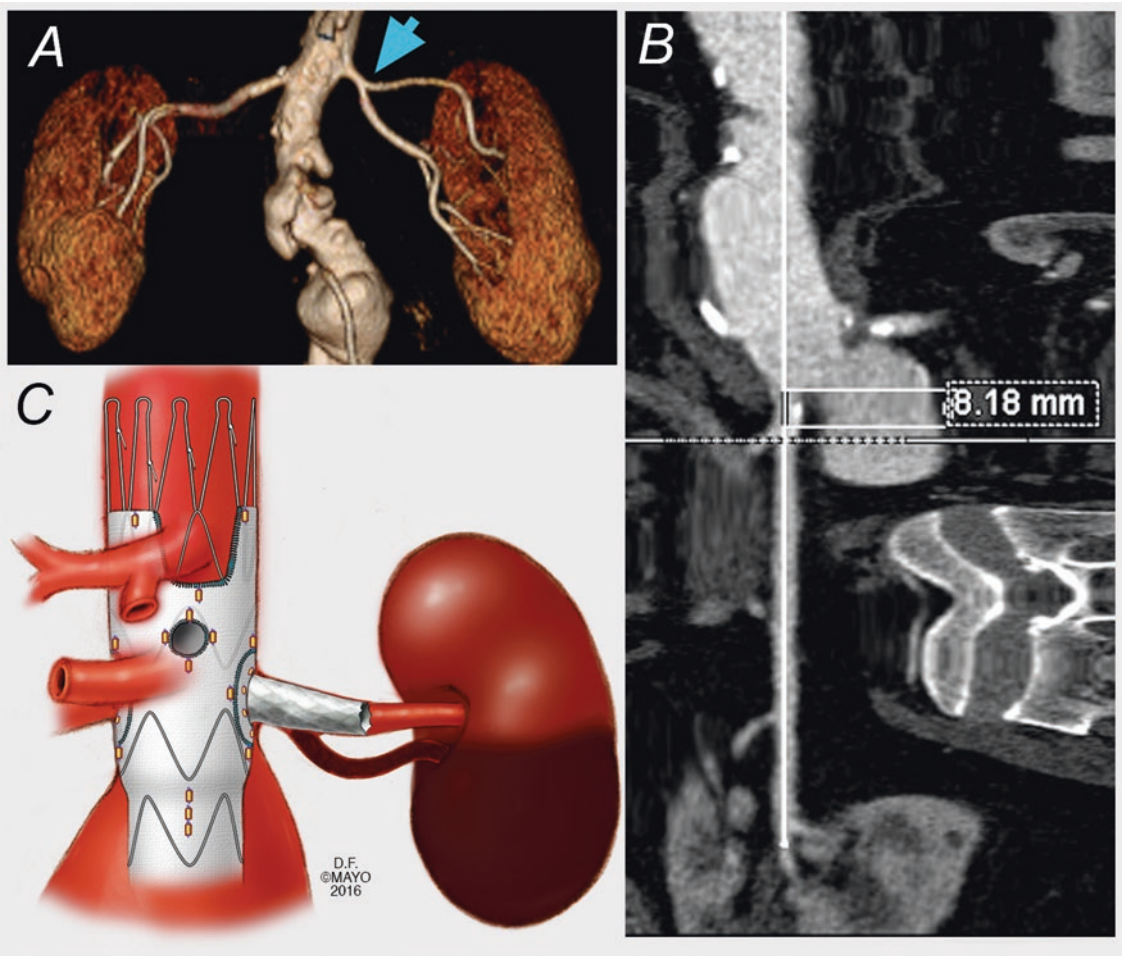

Fig. 11.12 Branch vessel analysis is critical to plan these procedures. Computed tomography angiography of a patient with juxta-renal aortic aneurysms shows early bifurcation of the left main renal artery (**a**, *arrow*). This is measured using centerline of flow analysis (**b**). Branch vessel stenting in this patient would result in large infarct of the lower pole of the left kidney (**c**). By permission of Mayo Foundation for Medical Education and Research. All rights reserved

each aortic branch ostium and the proximal seal is then measured from the straightened view of the CLF, allowing precise calculation of the location of a fenestration in the longitudinal axis (Fig. 11.14). The straightened view of the CLF is then rotated such that the visceral segment is properly aligned with the vertebral bodies. Usually this means the superior mesenteric and celiac arteries are oriented anteriorly, and the renal arteries are directed laterally.

By assessing each imaging orthogonal to the CLF at the midpoint of the vessel origin, the radial position of the branch ostium can be described (Fig. 11.15). This is typically done as a clock position, angle (0°–360°), or it can be more accurately described as an arc length from the 12:00 o'clock position. Figure 11.16 summarizes the sequence of measurements for planning definitive repair. Most common factors limiting suitability of repair are multiple small renal arteries, excessive angulation, early vessel bifurcation, and excessive atherosclerotic debris (Fig. 11.17).

Surveillance Protocols

Surveillance using periodic cross-sectional imaging remains an essential part of continued care after endovascular aortic repair. In the setting of open surgery, baseline imaging is obtained to establish the appearance of the aorta following the repair, in addition to the presence or absence of concurrent arterial disease. More specific questions are raised after an endovascular aortic repair. Potential problems include stent migration, the presence of endoleaks into the aneurysm sac, and the integrity of the prostheses form.

Follow-up CTA studies include typically a pre-contrast, contrast, and delayed phase. The pre-contrast image provides information on regions of calcification that may be confused with endoleaks and the relationship and metallic integrity of all modular stent-graft components. If there are specific questions about the graft integrity, the source CT data can be

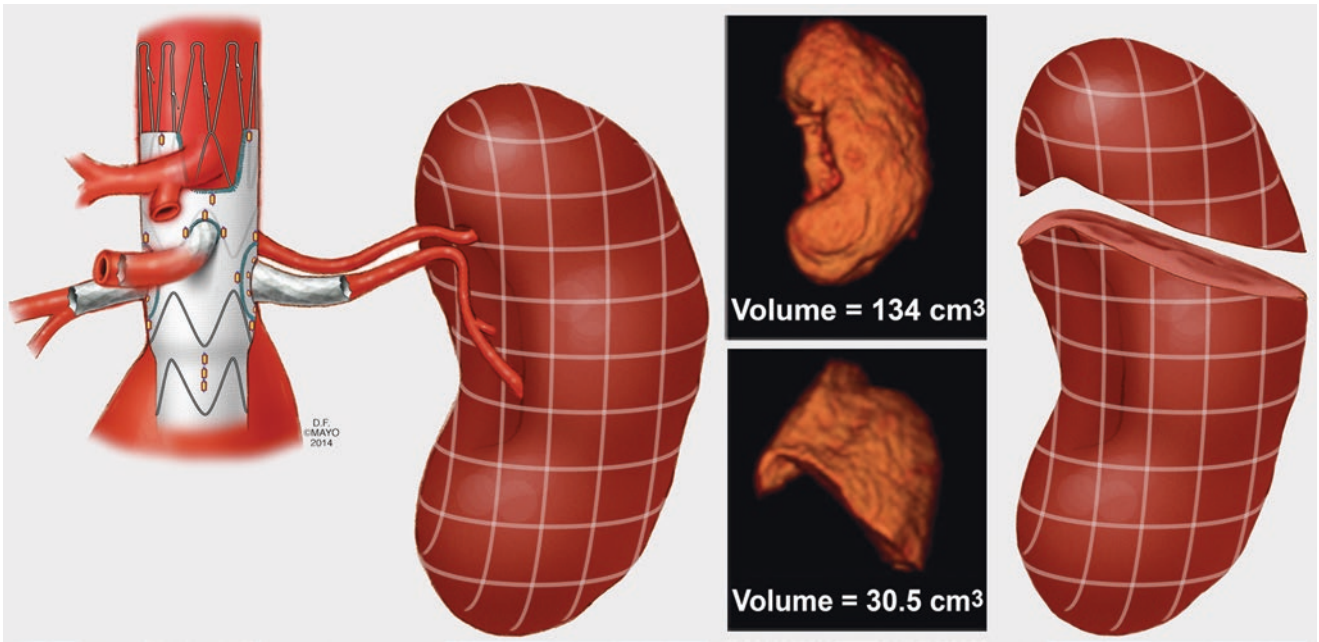

Fig. 11.13 Technique of volumetric analysis in patients with early renal artery bifurcation has been used to select patients for branch vessel stenting. By permission of Mayo Foundation for Medical Education and Research. All rights reserved

reconstructed using alternative algorithms. During the post-processing analysis, a hardware mask can be applied to the data set to help illustrate the metallic structures involved in the repair. Contrast studies are used to assess endoleak, migration, stenosis, occlusion, or thrombus. The timeline of potential problems that can occur after fenestrated and branched repair is summarized in Fig. 11.18. Endoleak assessment requires review of the contrast phase images side-by-side as compared to the pre-contrast images so that the patterns of calcification will not be confused with endoleaks. The CLF model is used to assess the maximal aortic diameter and to calculate aneurysm volume. The delayed phase studies are used to assess the sac for subtle evidence of endoleak. This is best done by comparing two or three of the phases of the studies side-by-side in assessing the HU in any area of question.

Although surveillance paradigms have evolved for standard EVAR from routine CTA to duplex ultrasound, fenestrated and branched endografts continue to be followed using a rigid regime. This is largely explained by its investigational nature and by the potential risk for other failure mechanisms involving not only the main aortic component but its side branches. Therefore, we continue to recommend a CT/CTA at dismissal, within 1–2 months, 6 months, and yearly thereafter. Duplex ultrasound is performed to assess side branch patency in addition to CTA. There is considerable debate regarding the benefit of such extensive protocols after EVAR. One must remember that aside from the financial cost, there is exposure to radiation and contrast.

Endoleaks

Endoleak classification has been well established by the reporting standards of the SVS for standard EVAR. Although this classification has not been officially modified for more complex repairs, an ongoing SVS taskforce headed by the author is proposing a new classification system to address additional sites of endoleak that can occur with fenestrated, branched, and parallel stent-grafts (Fig. 11.19). This classification maintains the standard definitions of Type Ia (Figs. 11.20, 11.21, and 11.22), Ib, II, and IV endoleaks. However, it adds detail pertinent to side branch involvement such as type Ic endoleak (Figs. 11.23 and 11.24), which is defined by an endoleak originating from the sealing site of a branch stent or fenestration. In addition, Type III or inter-component endoleak (Figs. 11.25 and 11.26) is further classified to address the specific origin. As such, Type IIIa endoleak specifies the attachment of the fenestrated and branch component with its bifurcated device, IIIb iliac limb and IIIc side branch component endoleaks (Fig. 11.27). Type IIId endoleak occurs due to integrity issues such as tear, perforation or fracture in the stent-graft or branches (Fig. 11.28).

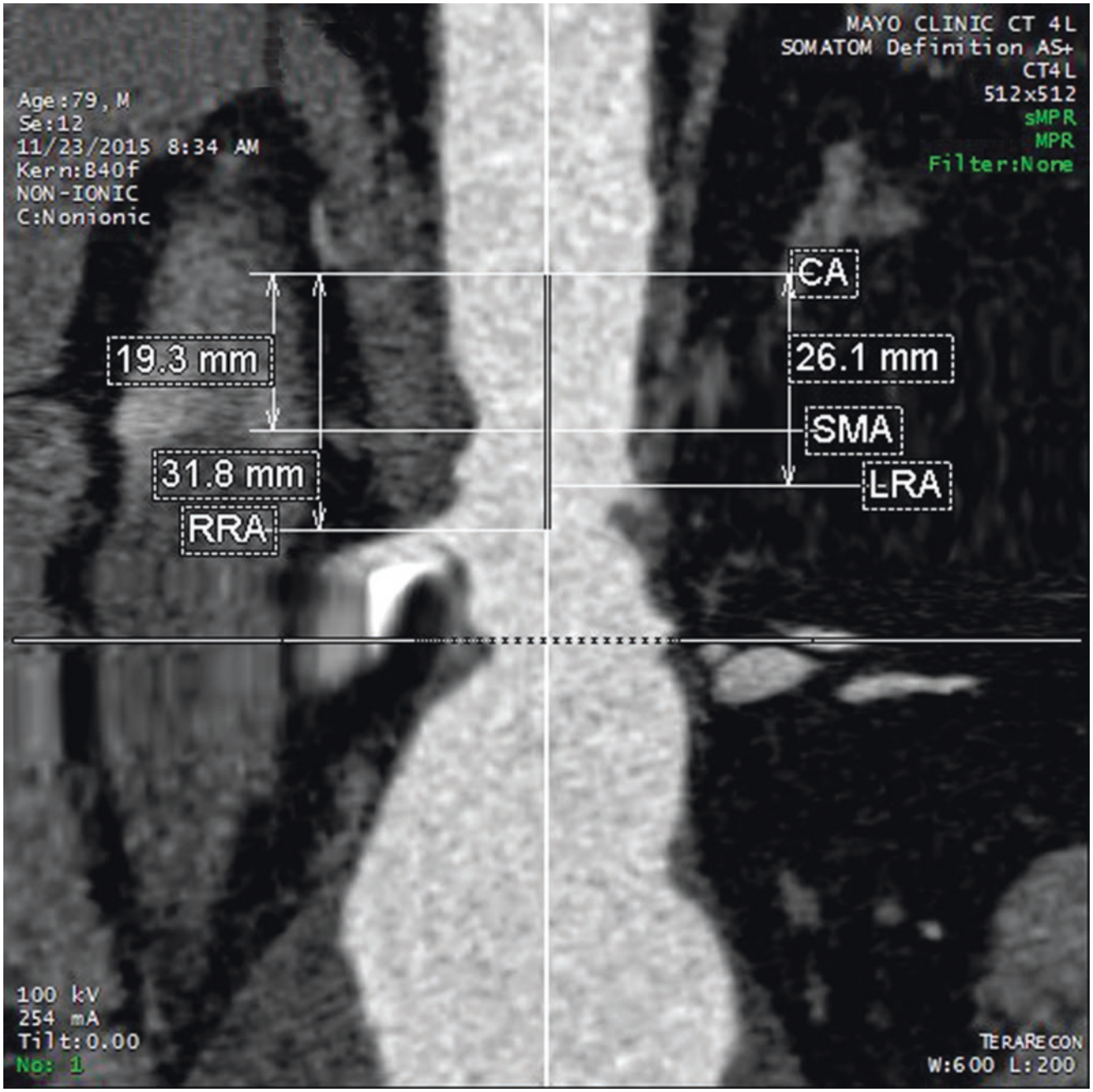

Fig. 11.14 After selection of a healthy landing zone in a patient with paravisceral aortic aneurysm, lengths are measured between the each of the vessels. By permission of Mayo Foundation for Medical Education and Research. All rights reserved

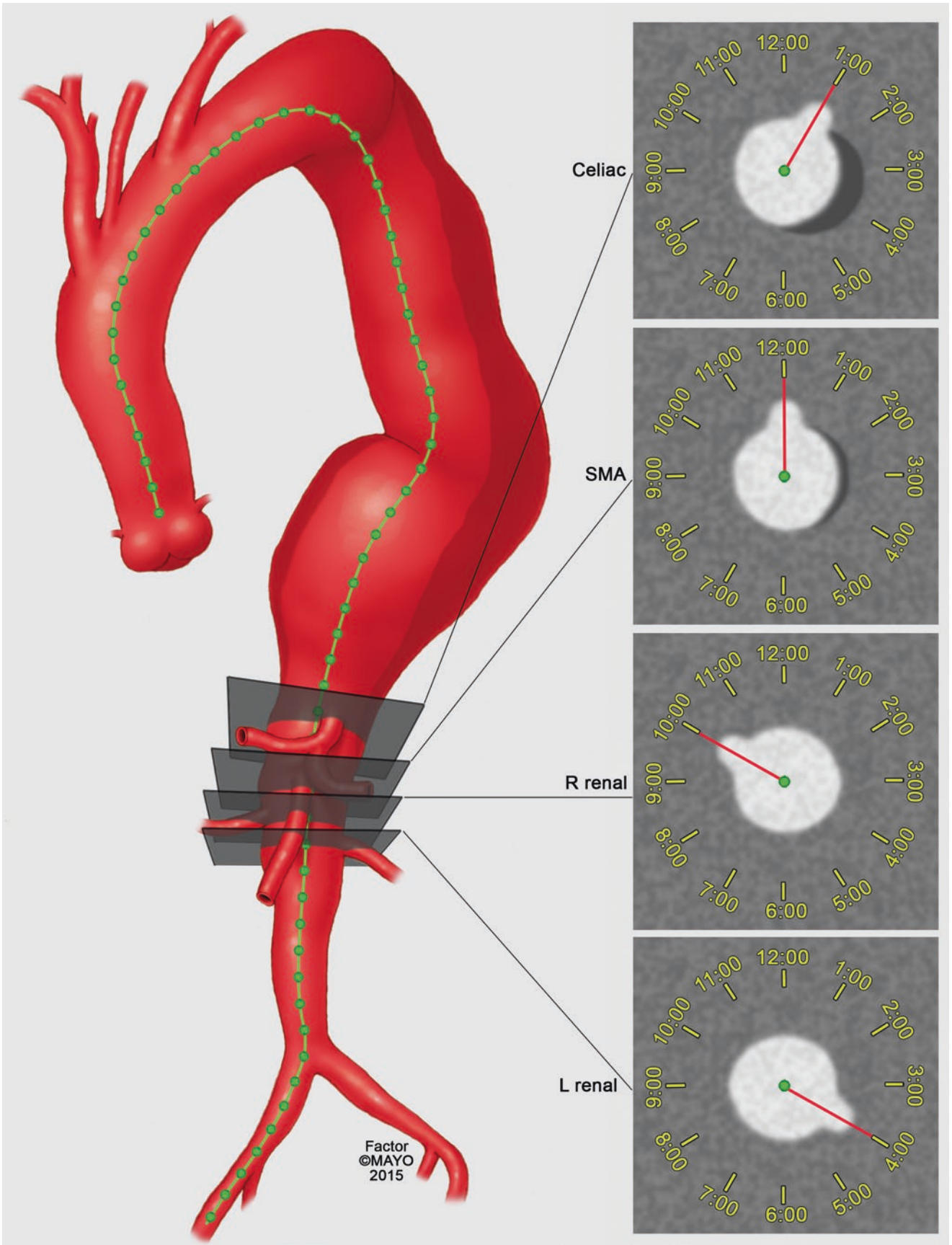

Fig. 11.15 Measurement of clock positions for the renal-mesenteric arteries. By permission of Mayo Foundation for Medical Education and Research. All rights reserved

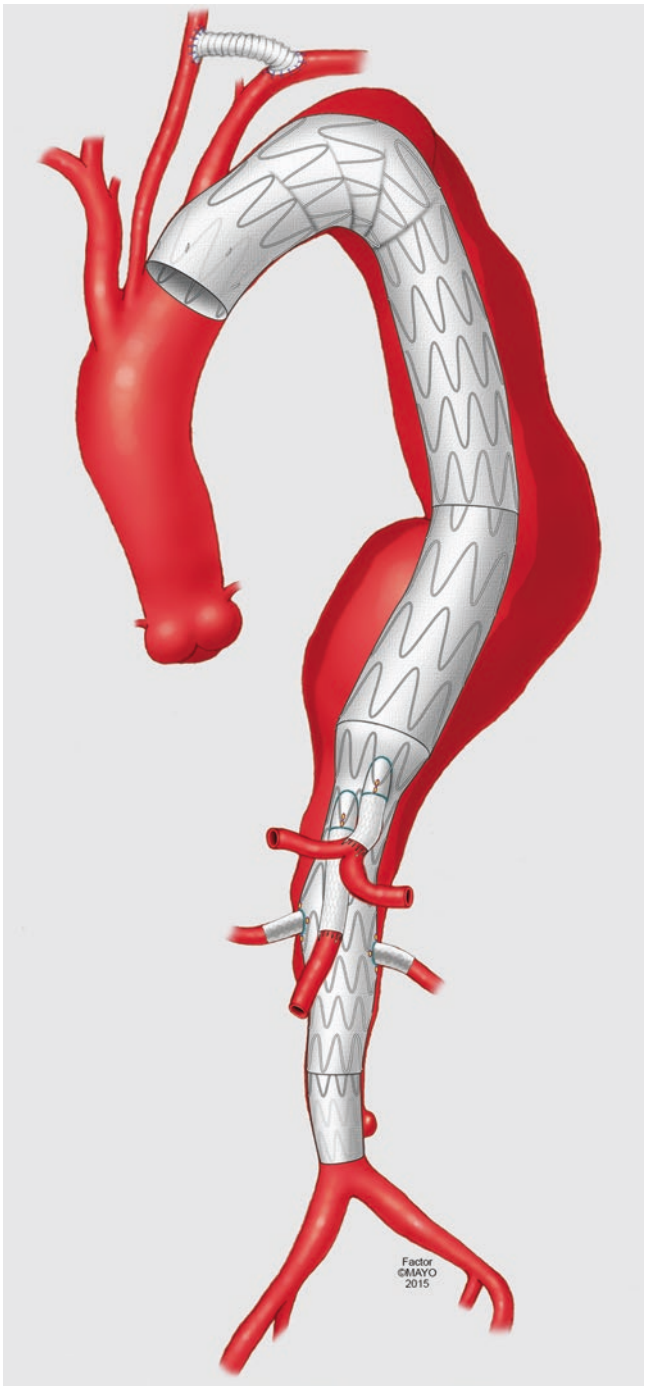

Fig. 11.16 Summary of sequence of measurements for planning fenestrated and branched endovascular repair in a patient with type I thoracoabdominal aortic aneurysm. By permission of Mayo Foundation for Medical Education and Research. All rights reserved

Type IV endoleak is ubiquitous intra-operatively and usually resolves with reversal of anticoagulation. Finally, specific mechanisms of branch-related endoleaks are also clarified in the classification.

Branch Stenosis, Kink, or Occlusion

Placement of side branch stents to incorporate the renal-mesenteric arteries is associated with potential risk of stenosis or occlusion from kinks, intimal hyperplasia, thrombus formation, or atherosclerotic disease. Assessment of side branch stenosis by CTA alone can be difficult because of extensive metallic artifact (Fig. 11.29) for stainless steel stents and numerous radiopaque markers. For fenestrated alignment stents, the leaflets of the stent should be flared into the aortic lumen, protruding 2–5 mm (Figs. 11.30 and 11.31). Compression of the stent can result from intra-procedural maneuvers such as advancement of a large dilator to place an iliac limb extension (Figs. 11.32 and 11.33). Assessment of the side branches by CT may help prevent avoidable occlusions from unrecognized stent compression. In patients with scallops not aligned by stents, the ostia of the vessel should be assessed for fabric coverage which can result in occlusion or branch malperfusion (Fig. 11.34). Finally, intimal hyperplasia is a common cause of stent stenosis in bare metal stent segments as depicted in Figs. 11.35 and 11.36.

Solid Organ Embolization

Embolization of atherosclerotic debris, plaque, or thrombus is a major source of morbidity and mortality after fenestrated and branched repair (Fig. 11.37). Ribeiro and associates created a score system to assess the impact of atherosclerotic debris on embolic events (Fig. 11.38). Using this classification, presence of higher thrombus burden was associated with renal function deterioration and solid organ embolization in the liver, spleen and kidneys.

Component Separations

Inter-component separation can occur in any of the modular joints, including the side branches (Fig. 11.39), the fenestrated and distal bifurcated stent (Fig. 11.40) or the iliac limbs. Because the fenestrations and iliac limbs represent fixation points that relatively resistant to migration, the junction of the bifurcated distal stent and fenestrated stent is particularly susceptible to component separation.

Stent Infolding

Aortic stent-grafts are typically oversized 10–20 % relative to its intended aortic diameter. For fenestrated grafts the landing zone is typically selected at the level of the celiac

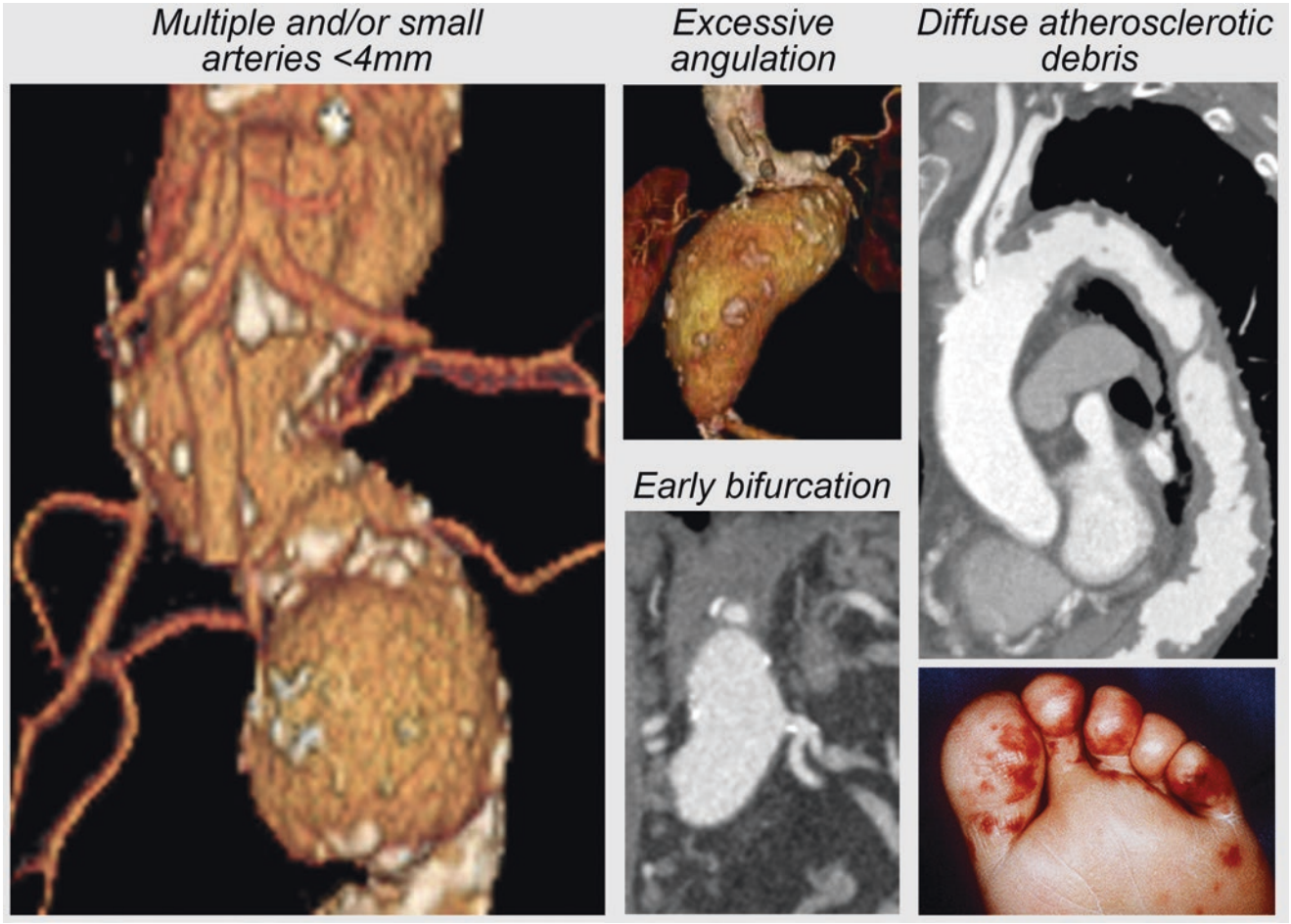

Fig. 11.17 Factors limiting suitability for fenestrated and branched endovascular repair. By permission of Mayo Foundation for Medical Education and Research. All rights reserved

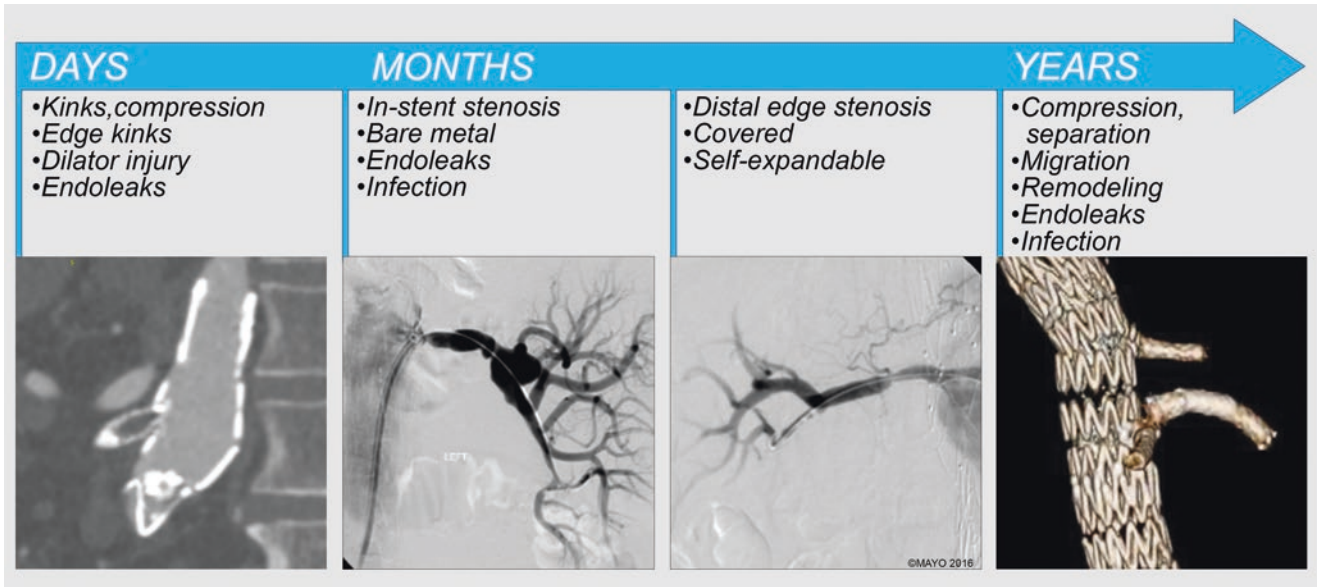

Fig. 11.18 Timeline of failure mechanisms for fenestrated and branched endovascular repair. By permission of Mayo Foundation for Medical Education and Research. All rights reserved

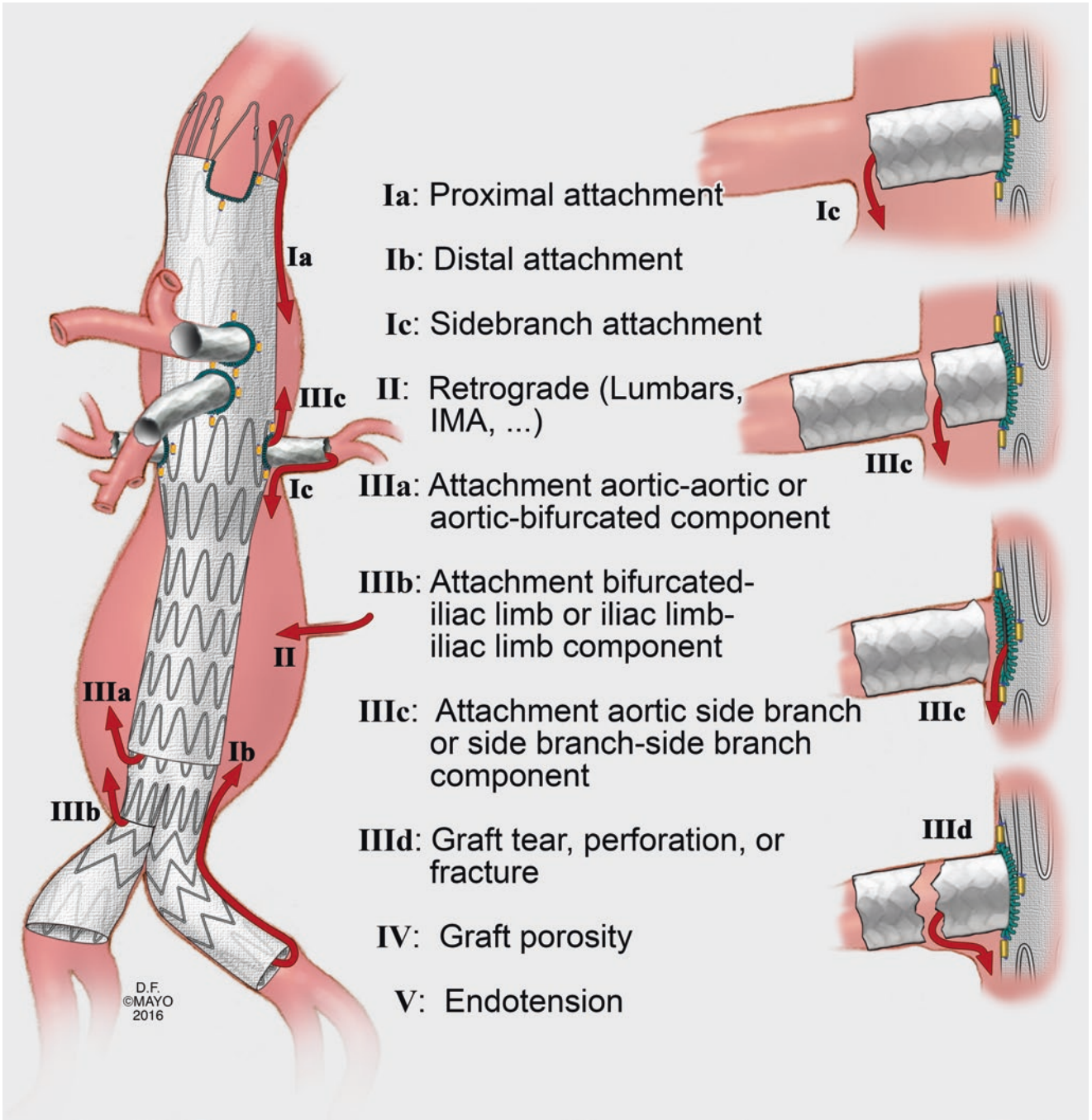

Fig. 11.19 New proposed classification for endoleaks in patients with complex aortic repairs. By permission of Mayo Foundation for Medical Education and Research. All rights reserved

axis, and there may be significant discrepancy in diameter relative to the renal arteries. Excessive oversizing around the renal arteries may predispose to stent infolding (see Fig. 11.21), which is a relatively infrequent complication but can lead to type Ia endoleak and branch compromise.

Progression of Aortic Disease

Aortic disease progression may be a cause of migration or loss of seal in the proximal landing zone (Fig. 11.41). Although migration of fenestrated stents is relatively infrequent with

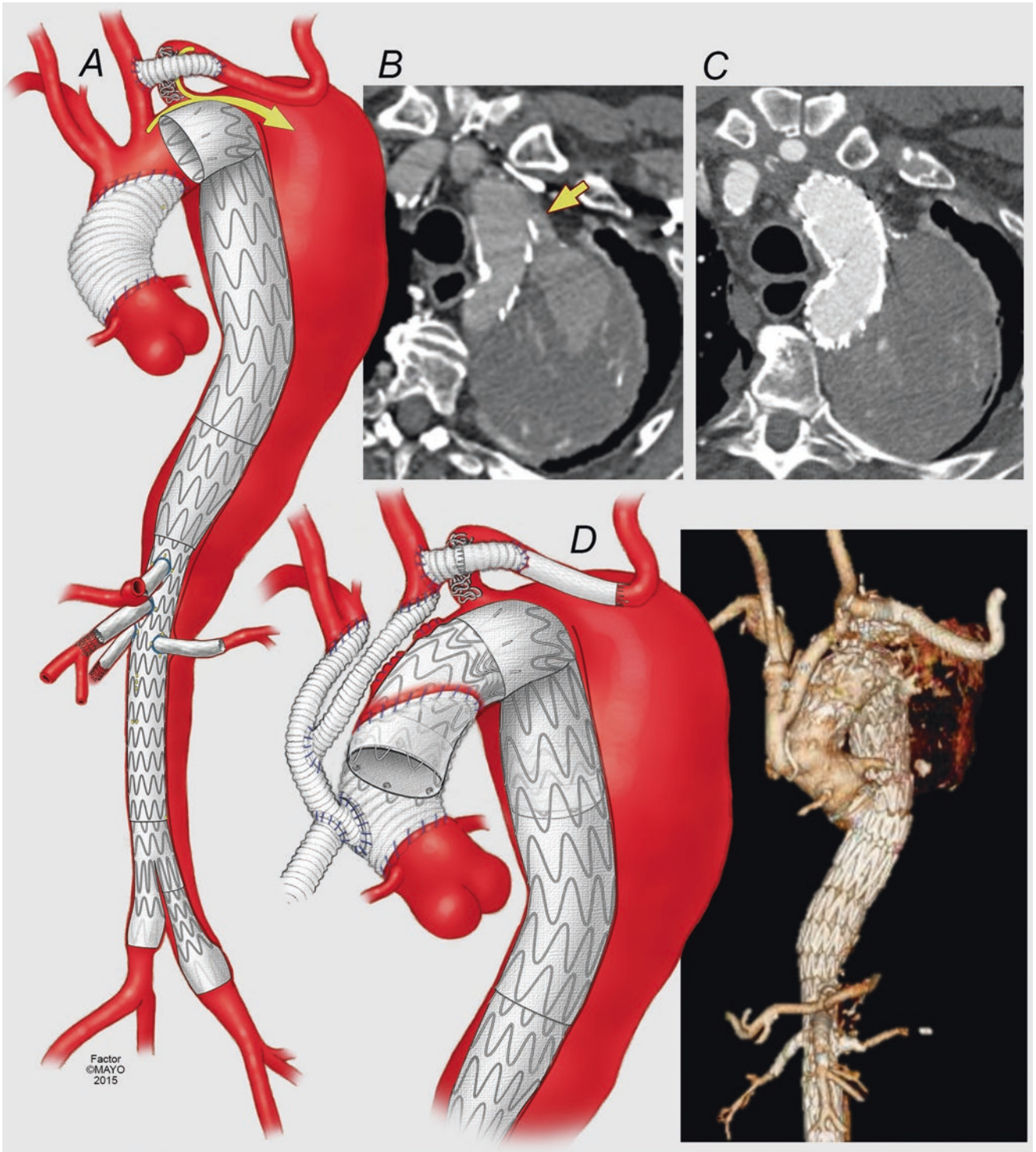

Fig. 11.20 Patient treated for chronic aortic dissection with a proximal Type Ia endoleak in the thoracic stent (**a**). Note the axial view of computed tomography angiography depicts lack of apposition between the stent-graft and aortic wall, indicative of Type Ia endoleak (**b**, *arrow*). The patient was treated by aortic arch debranching procedure (**d**), with resolution of the proximal endoleak. By permission of Mayo Foundation for Medical Education and Research. All rights reserved

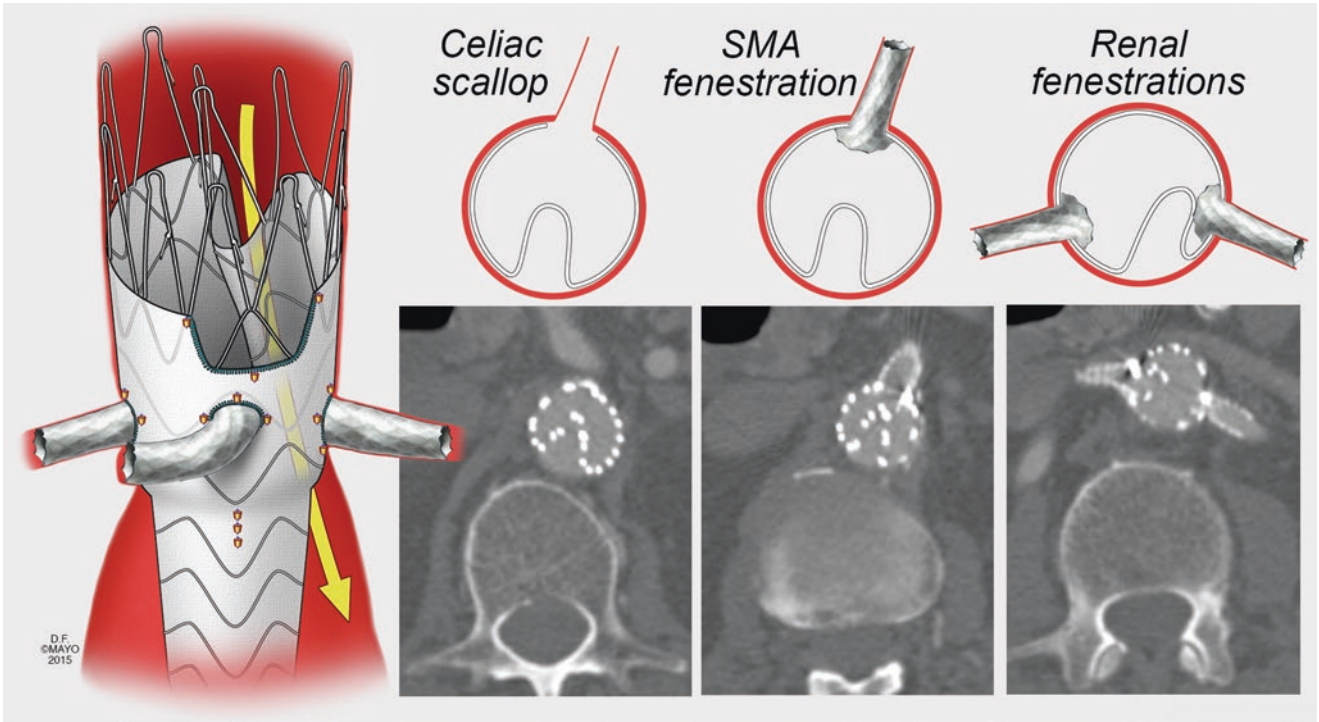

Fig. 11.21 Infolding of fenestrated stent-graft due to excessive oversizing caused a Type I endoleak. By permission of Mayo Foundation for Medical Education and Research. All rights reserved

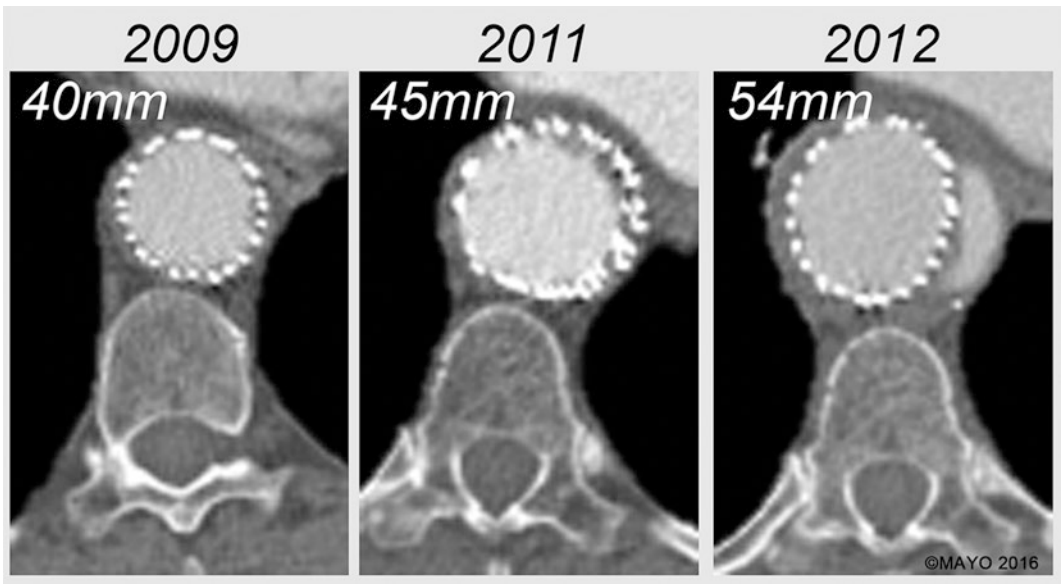

Fig. 11.22 Development of Type I endoleak due to progressive aortic disease affecting the proximal landing zone. By permission of Mayo Foundation for Medical Education and Research. All rights reserved

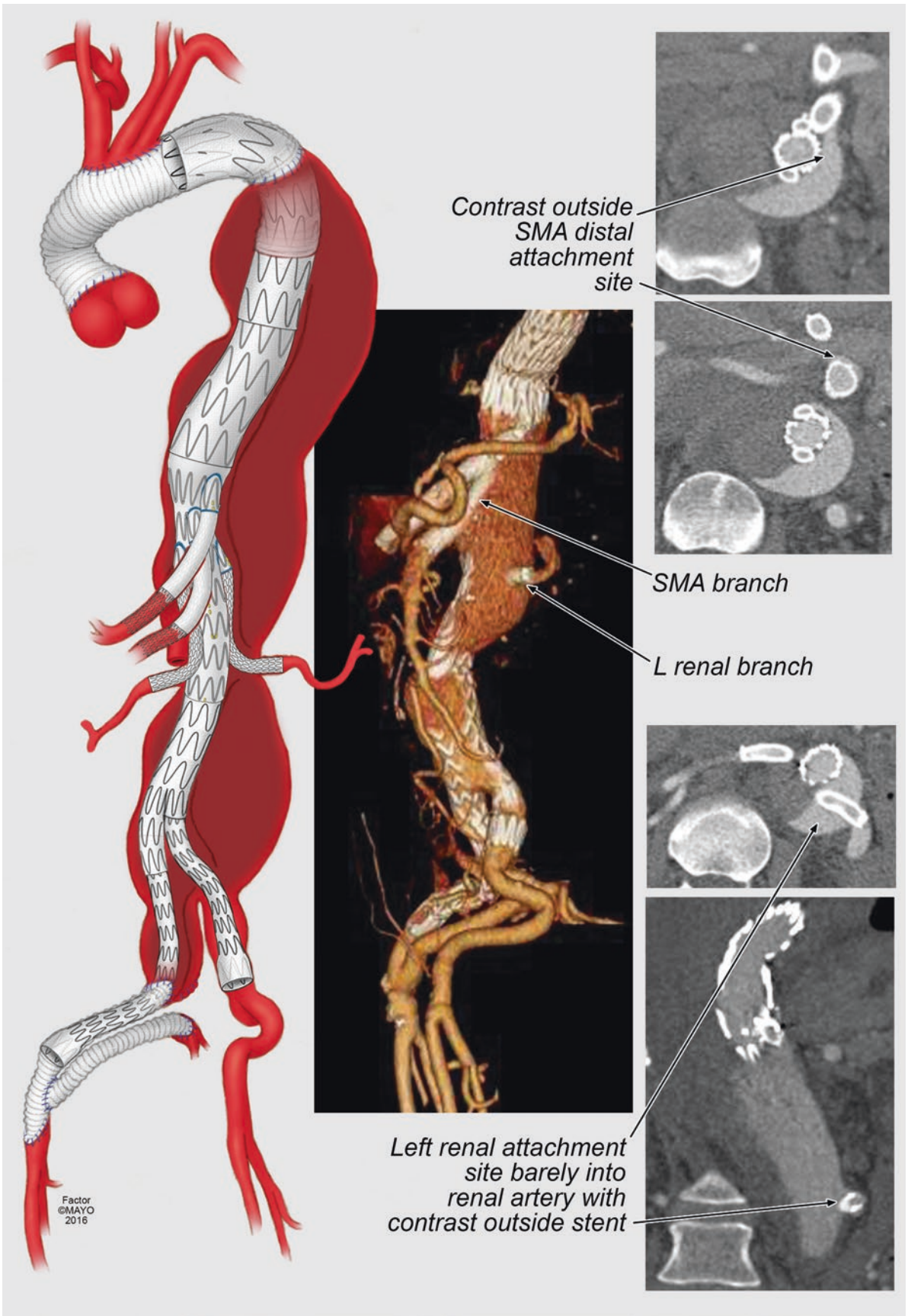

Fig. 11.23 Illustration of aortic repair in a patient with chronic dissection depicts a complex endoleak with origin from the distal sealing sites of the SMA and left renal stents (Type Ic). By permission of Mayo Foundation for Medical Education and Research. All rights reserved

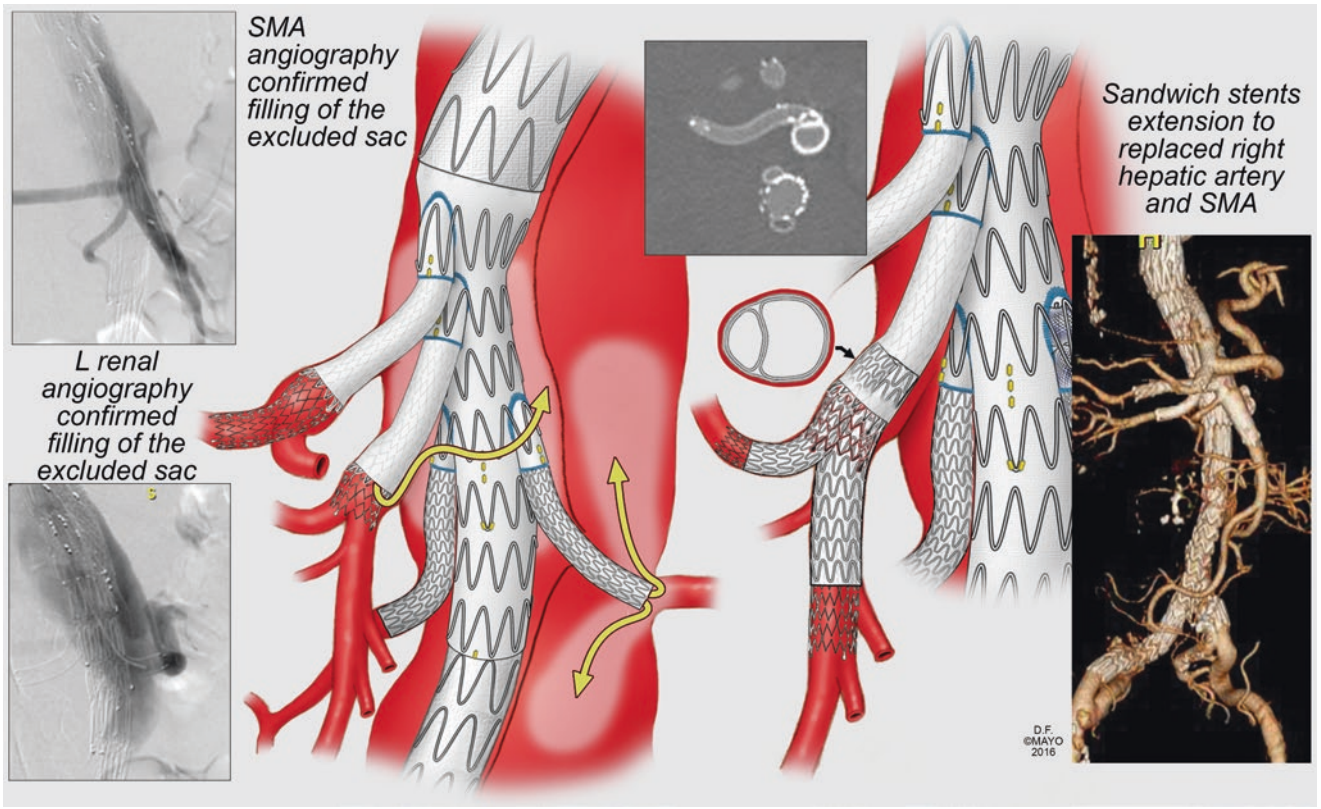

Fig. 11.24 Intraoperative angiography confirms Type Ic endoleak. Illustration depicts treatment by parallel branch graft in the SMA and occlusion of the left renal branch in this patient who was on chronic hemodialysis. By permission of Mayo Foundation for Medical Education and Research. All rights reserved

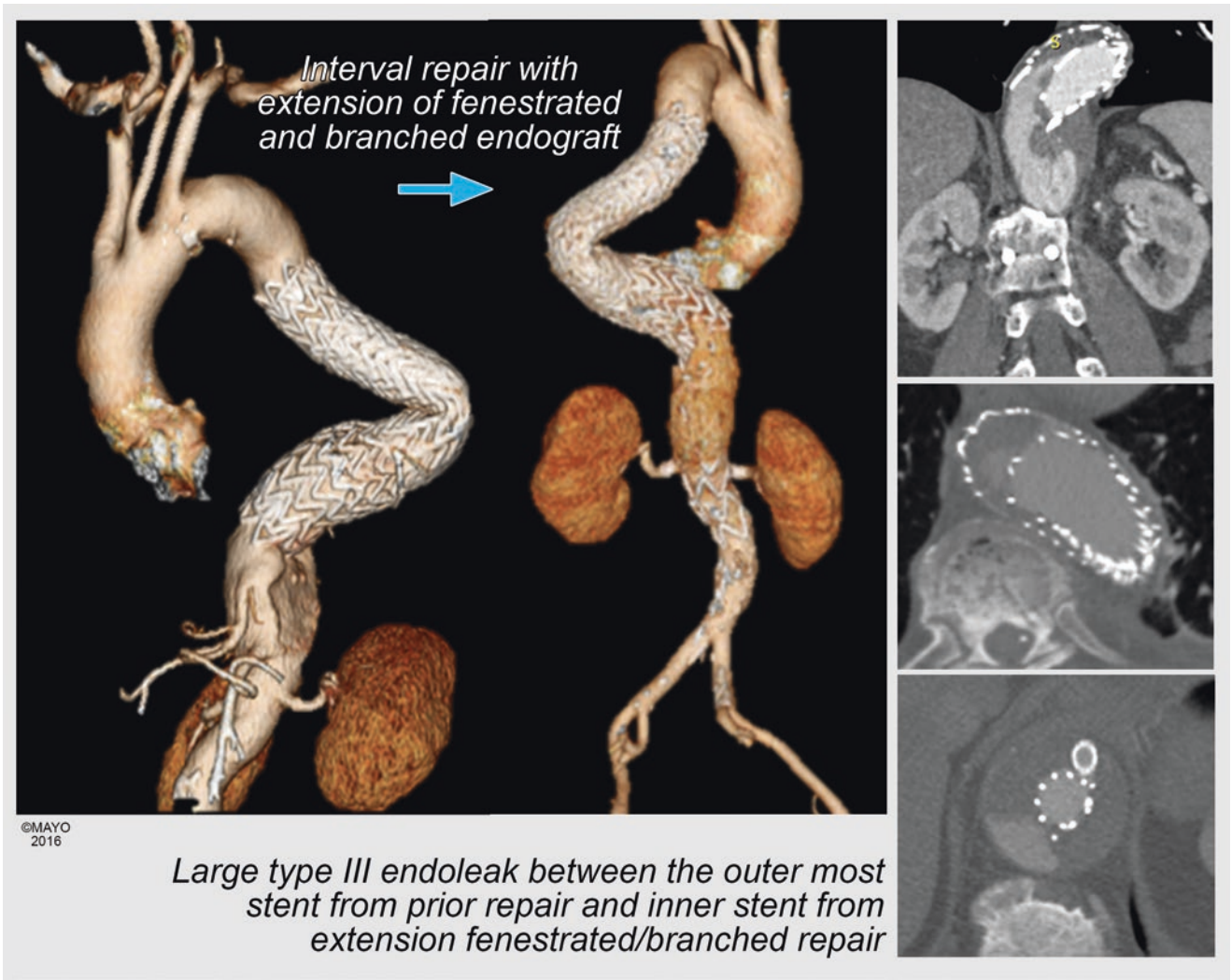

Fig. 11.25 Patient with prior thoracic endograft was treated by distal thoracoabdominal fenestrated–branched endograft with development of a large Type III endoleak at the overlap segment of the proximal and distal stents due to excessive tortuosity. By permission of Mayo Foundation for Medical Education and Research. All rights reserved

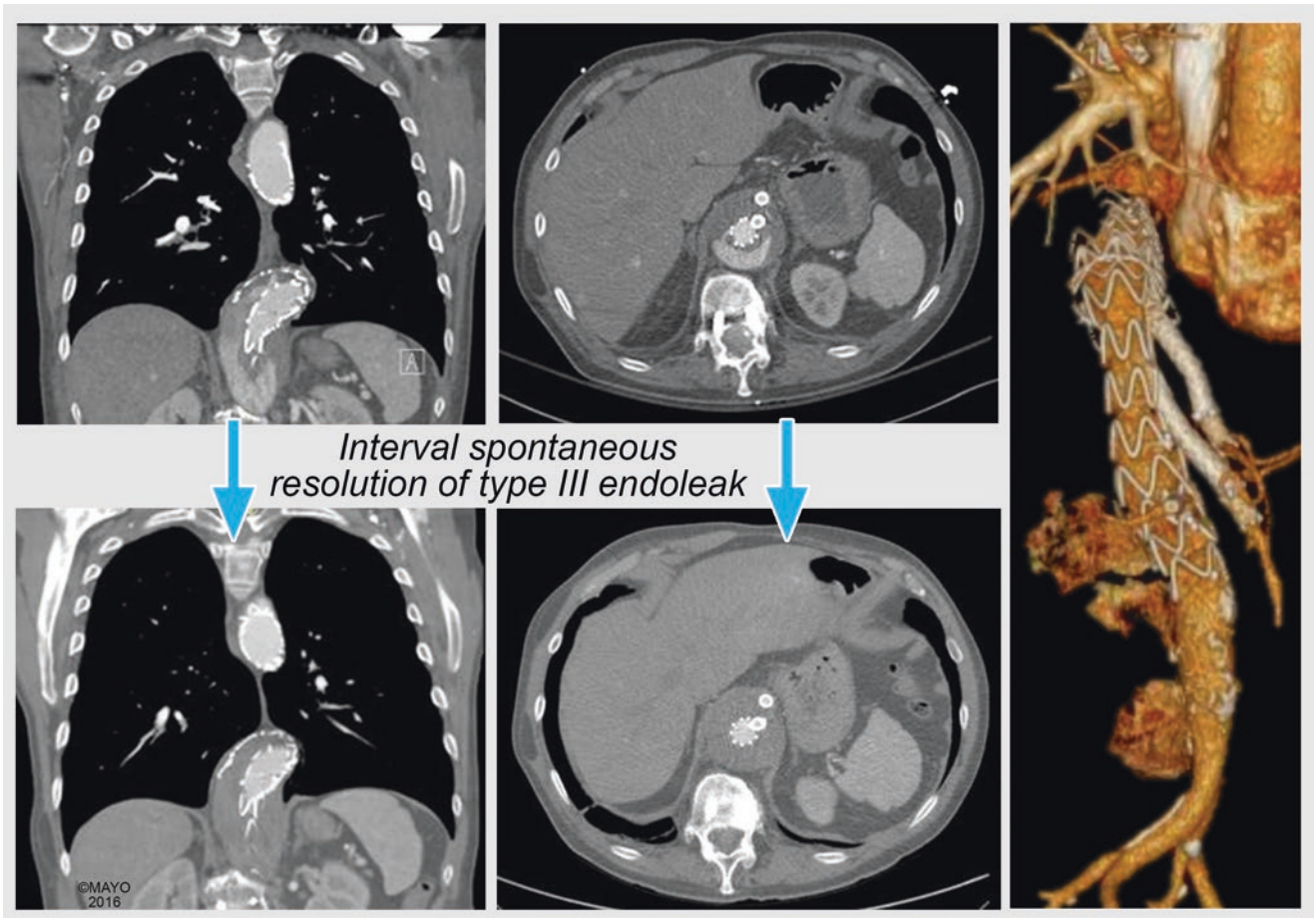

Fig. 11.26 Spontaneous resolution of the Type III endoleak depicted in Fig. 11.25. By permission of Mayo Foundation for Medical Education and Research. All rights reserved

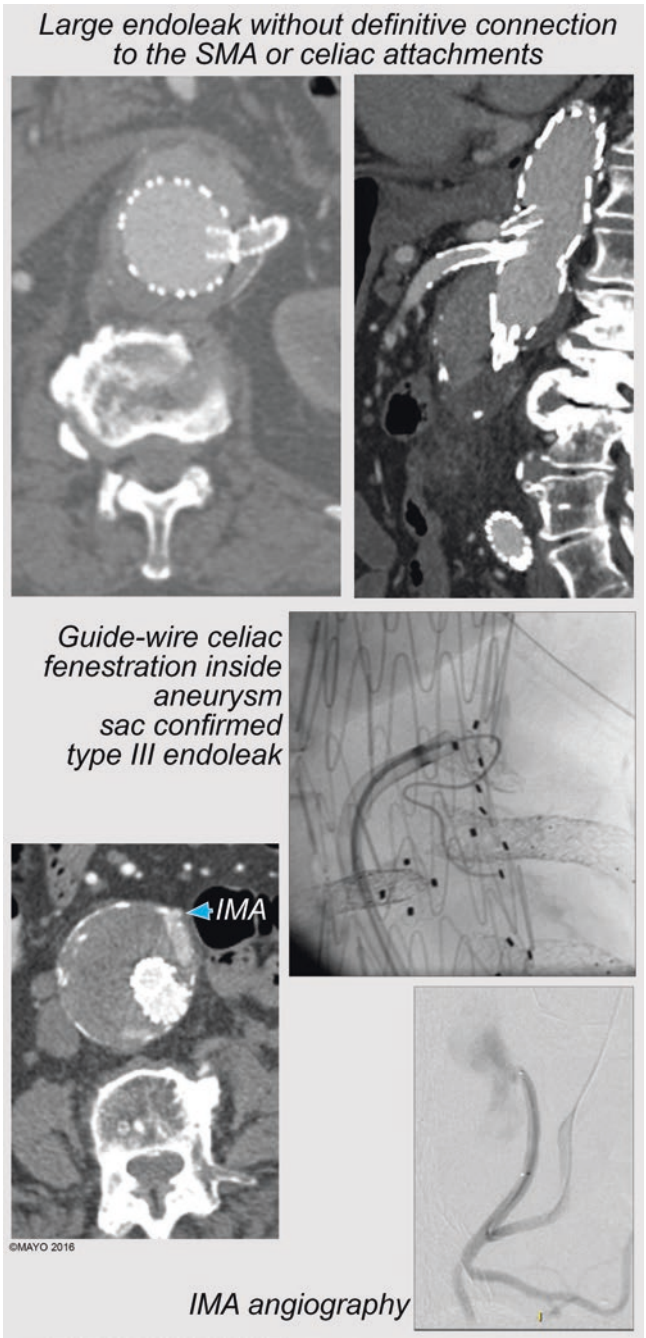

Fig. 11.27 Patient with type IIIc endoleak from the celiac fenestrated-branch. Note that the guide-wire exits through the fenestration. The patient also had a type II endoleak from the inferior mesenteric artery. By permission of Mayo Foundation for Medical Education and Research. All rights reserved

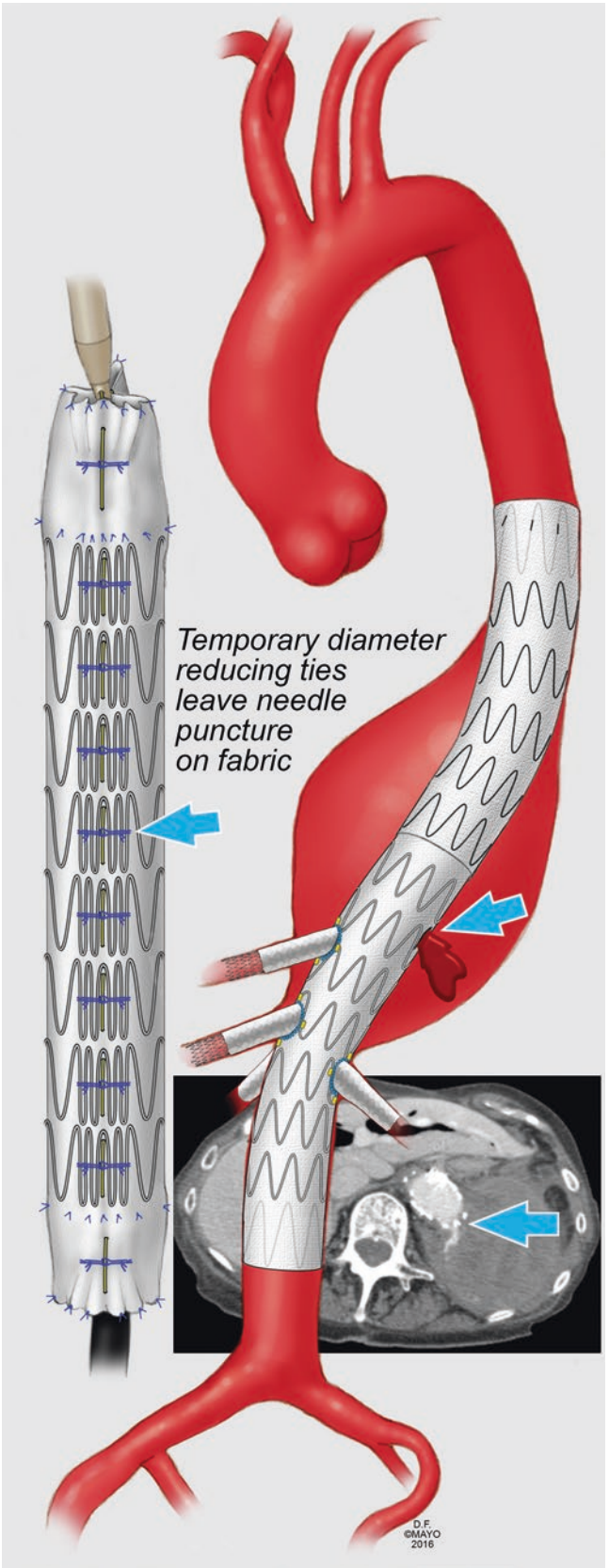

Fig. 11.28 Type IIId endoleak from fabric tear likely in the location of the diameter reducing ties. By permission of Mayo Foundation for Medical Education and Research. All rights reserved

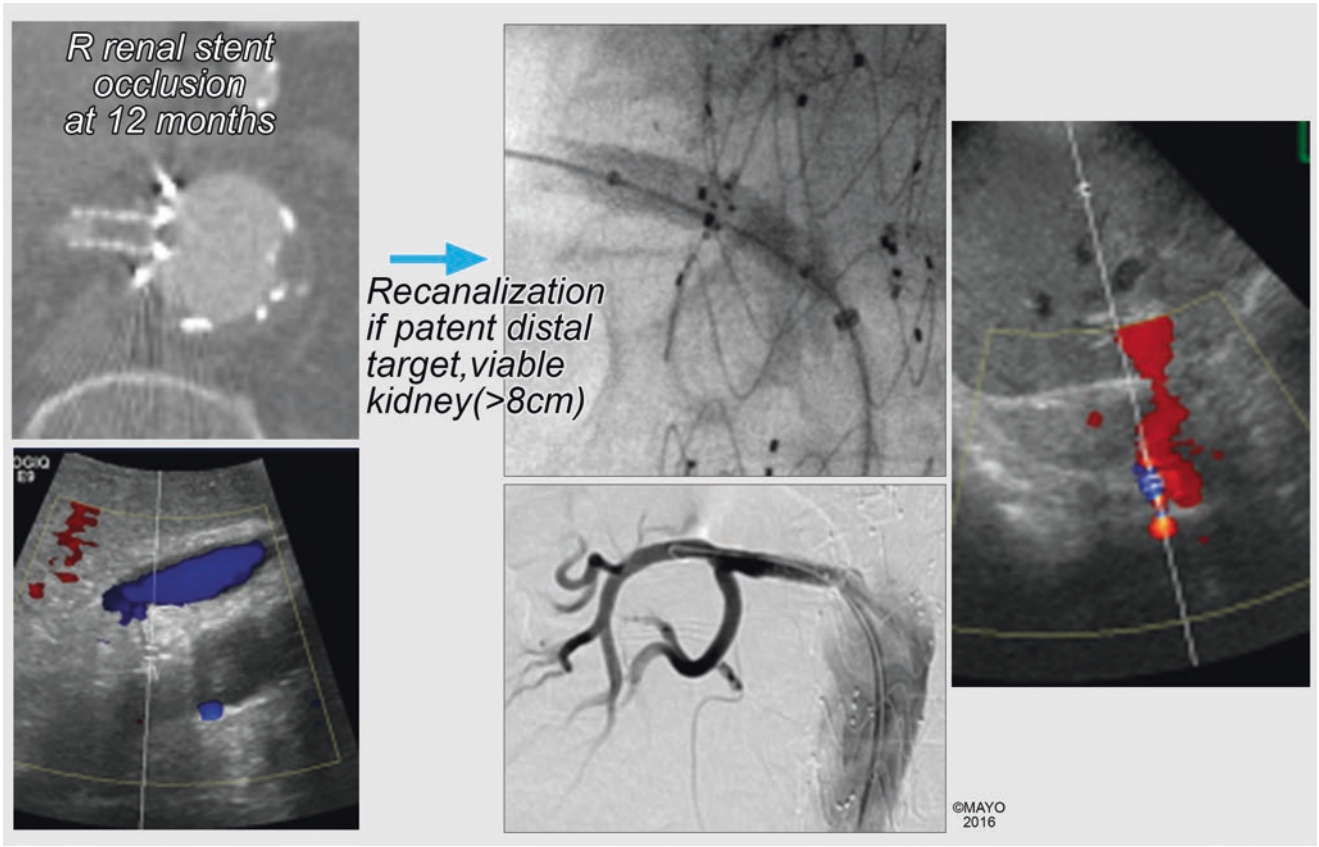

Fig. 11.29 Right renal artery occlusion is shown by CTA despite metallic artifact and is confirmed by duplex ultrasound. The patient was successfully treated by recanalization. By permission of Mayo Foundation for Medical Education and Research. All rights reserved

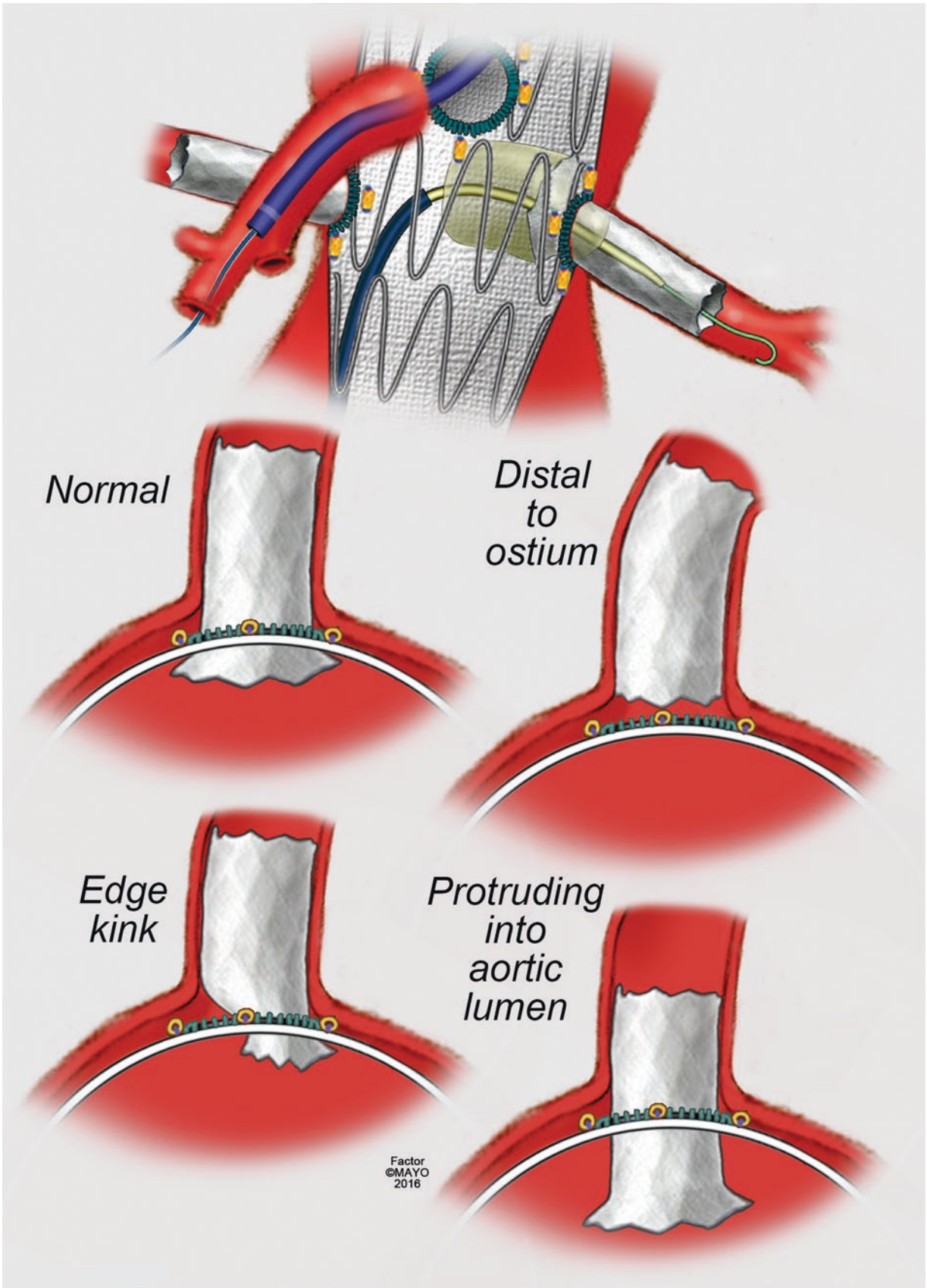

Fig. 11.30 The stent leaflets should be carefully evaluated by computed tomography angiography. These are flared with a large 10-mm balloon and should be located 2–5 mm into the aorta. Computed tomography angiography is critical to identify malposition and kink. By permission of Mayo Foundation for Medical Education and Research. All rights reserved

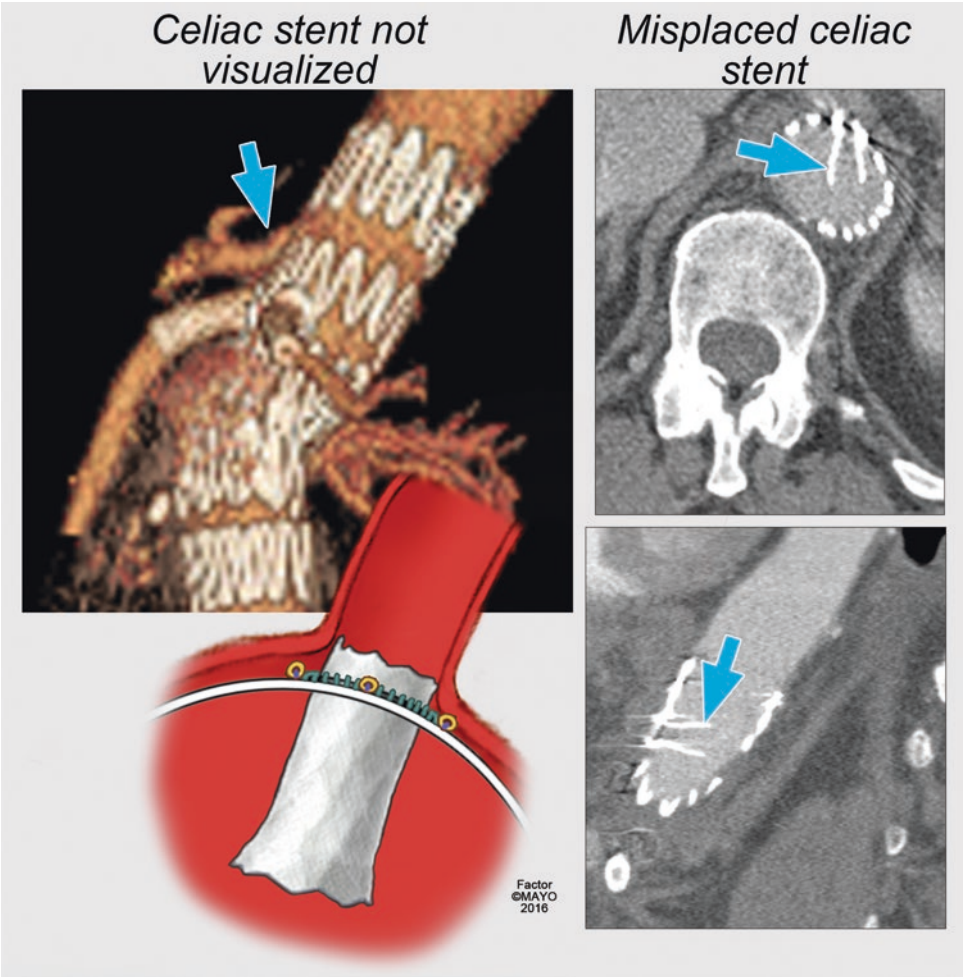

Fig. 11.31 The celiac stent migrated into the aortic lumen, likely during excessive flaring. This was detected by CTA and revised by removing the stent and relocating in one of the iliac limbs. The celiac artery was re-stented. By permission of Mayo Foundation for Medical Education and Research. All rights reserved

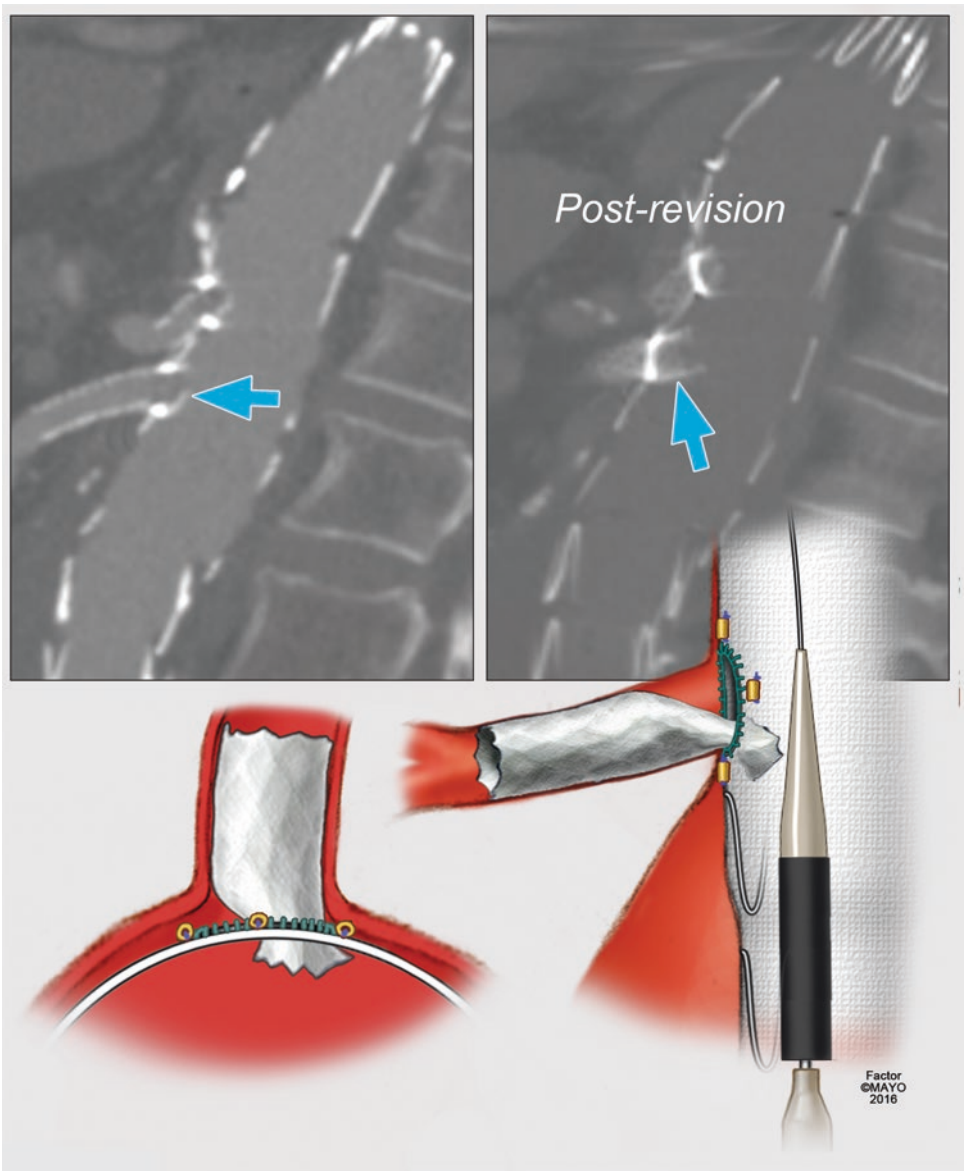

Fig. 11.32 The inferior leaflet of the stent is shifted upwards due to compression from the dilator tip. This was identified and revised with placement of additional stent and flaring. By permission of Mayo Foundation for Medical Education and Research. All rights reserved

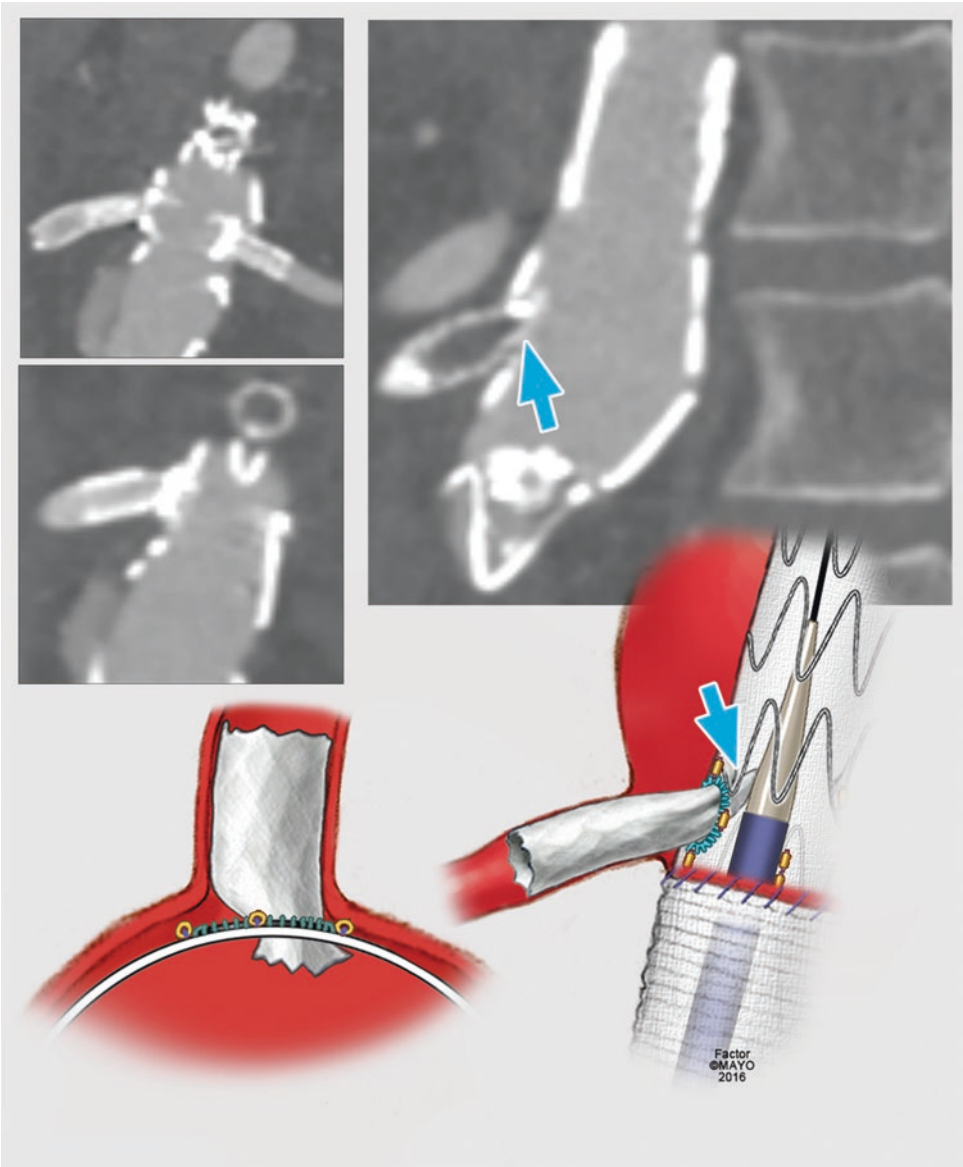

Fig. 11.33 Occlusion of the SMA stent also from compression by the dilator tip. This was successfully treated by recanalization of the stent. By permission of Mayo Foundation for Medical Education and Research. All rights reserved

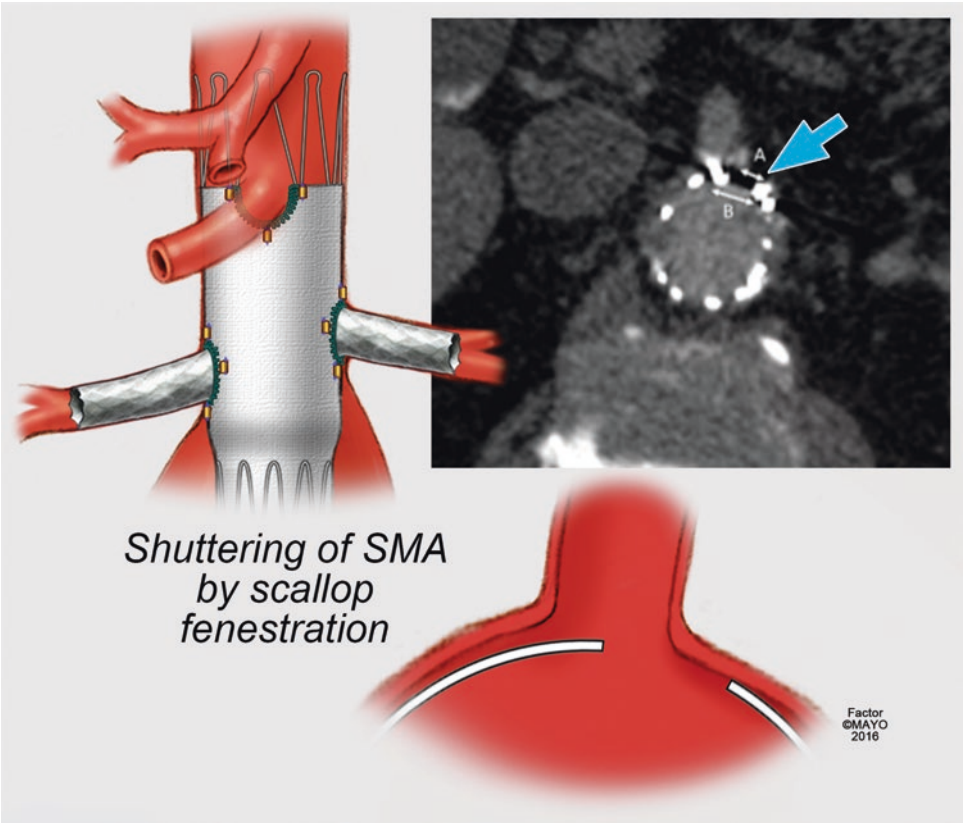

Fig. 11.34 Scallops are often not aligned by stent. It is important to evaluate shuttering of the origin of the vessel cause by misalignment of the scallop and target vessel. By permission of Mayo Foundation for Medical Education and Research. All rights reserved

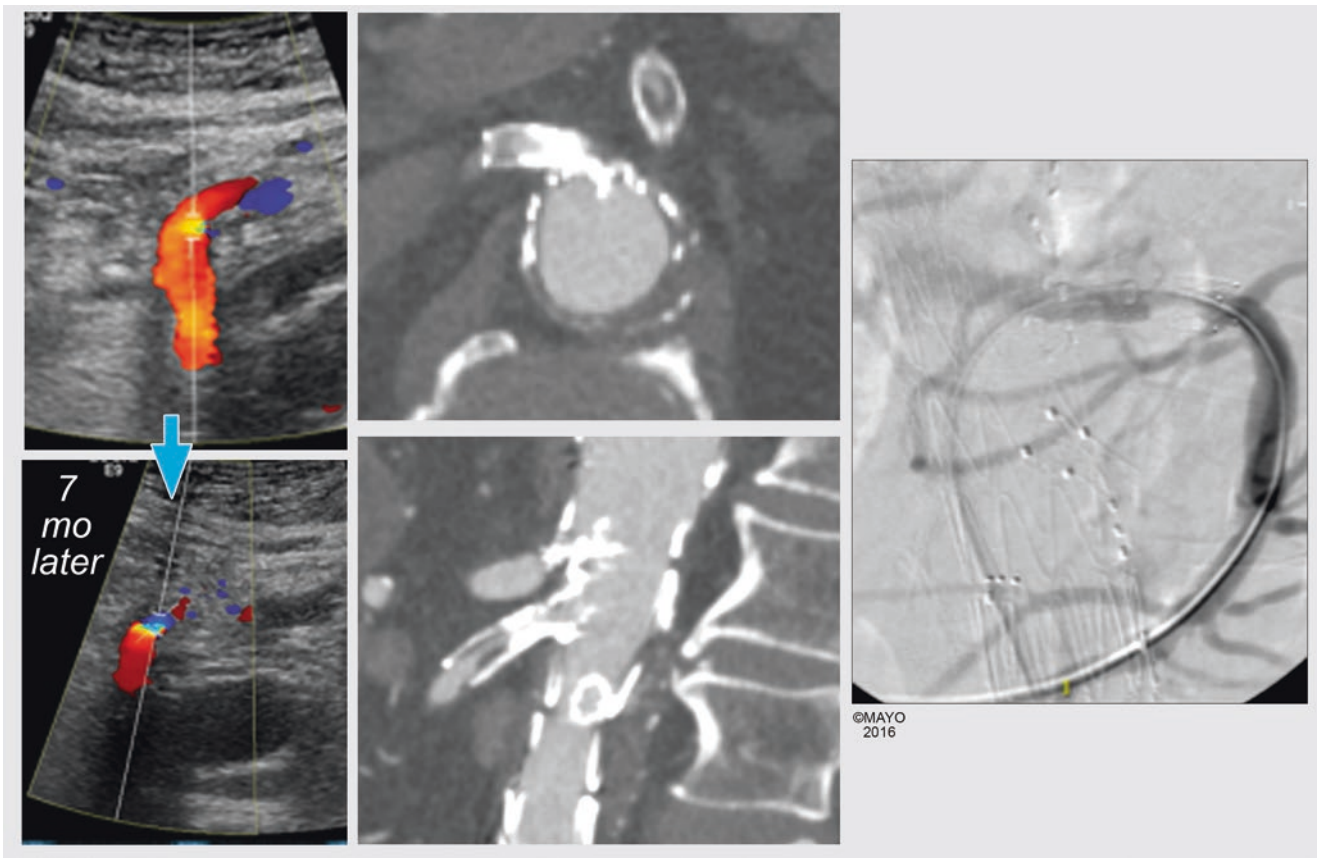

Fig. 11.35 Duplex ultrasound reveals high-grade stenosis of the stented SMA in the bare metal stent segment. This was confirmed by angiography and treated by redo stent placement. By permission of Mayo Foundation for Medical Education and Research. All rights reserved

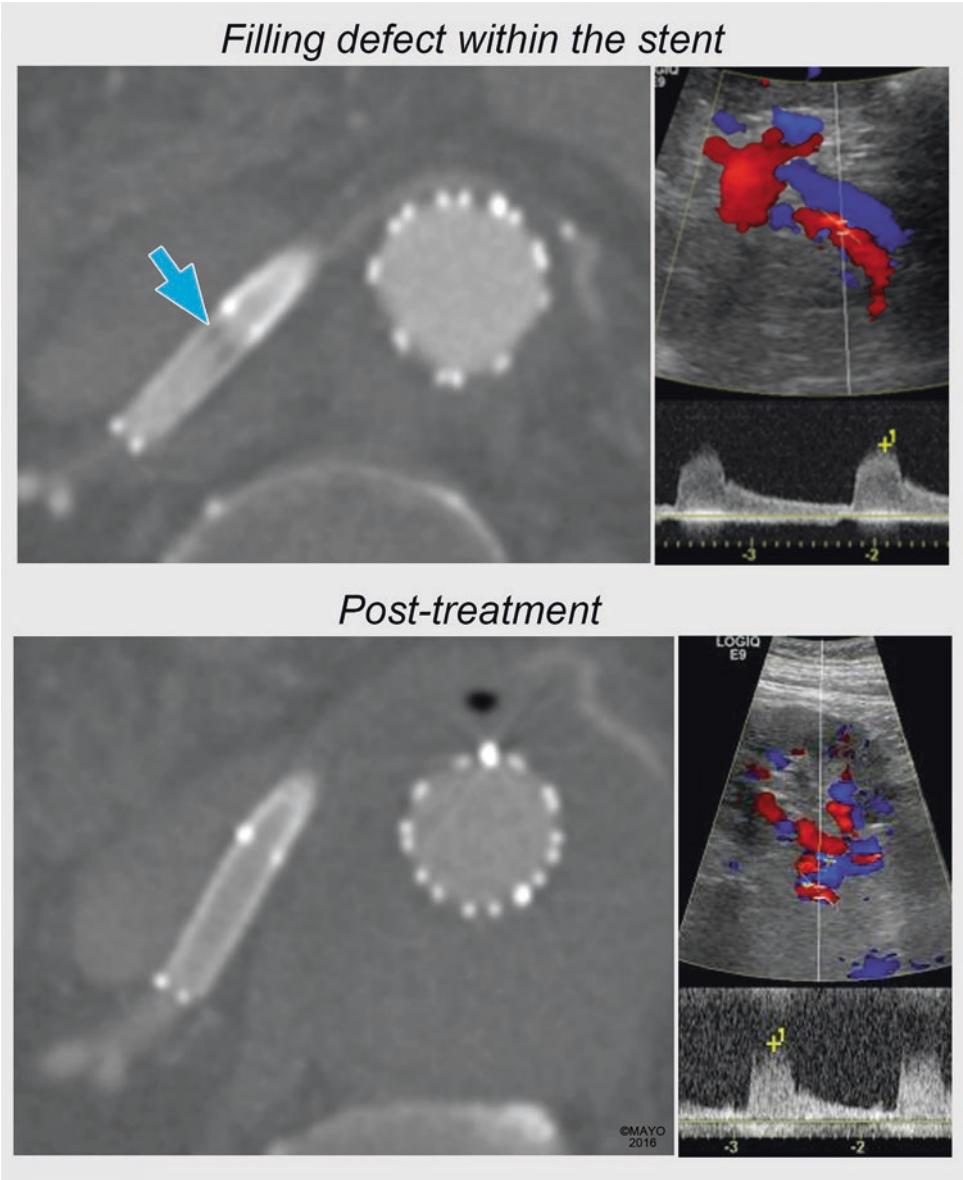

Fig. 11.36 Intimal hyperplasia causing stenosis of a right renal artery branch in the bare metal stent segment (*arrow*). This was successfully treated by placement of a self-expandable stent-graft. By permission of Mayo Foundation for Medical Education and Research. All rights reserved

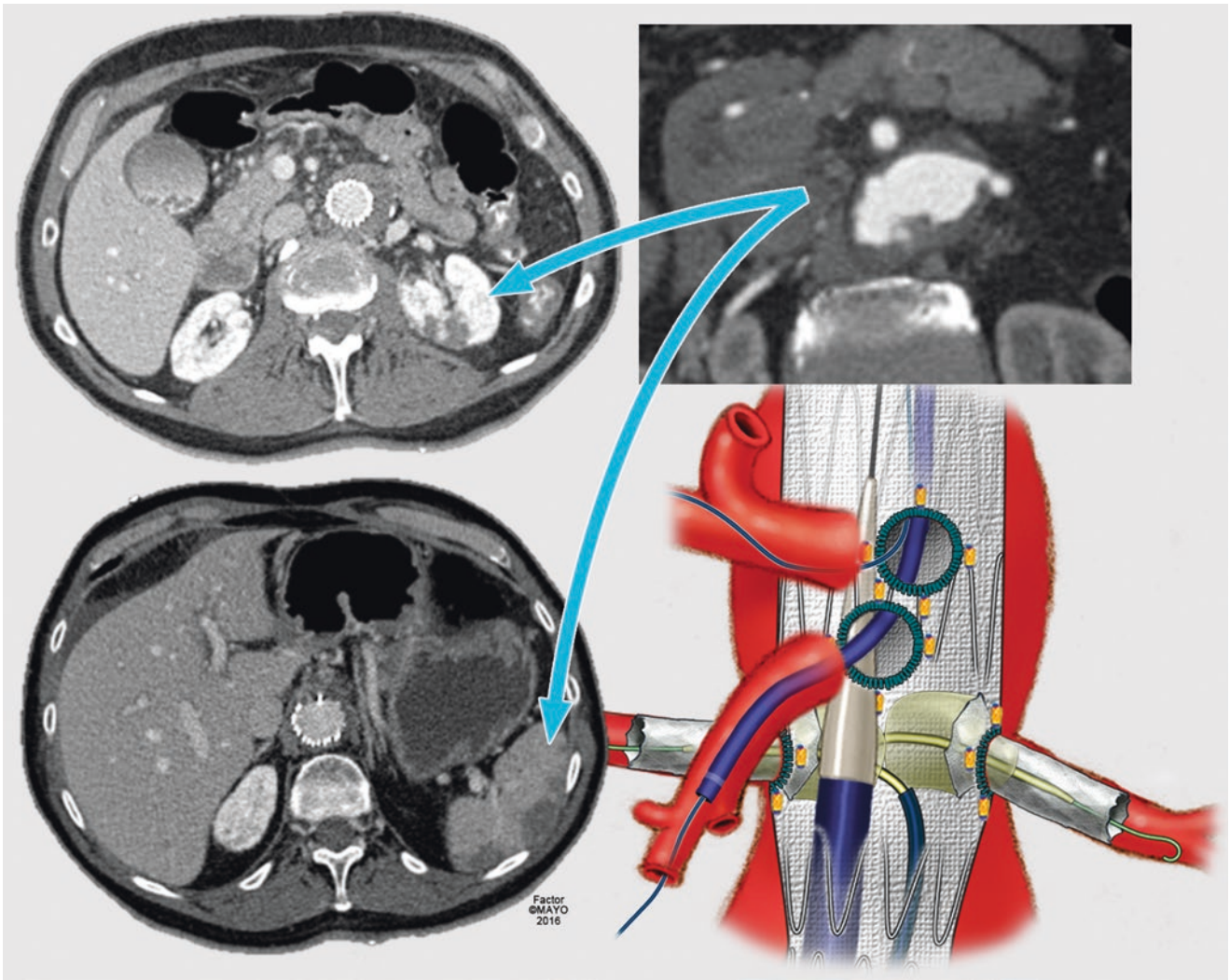

Fig. 11.37 Embolization to the kidney and spleen is noted on CTA in a patient with significant aortic debris. By permission of Mayo Foundation for Medical Education and Research. All rights reserved

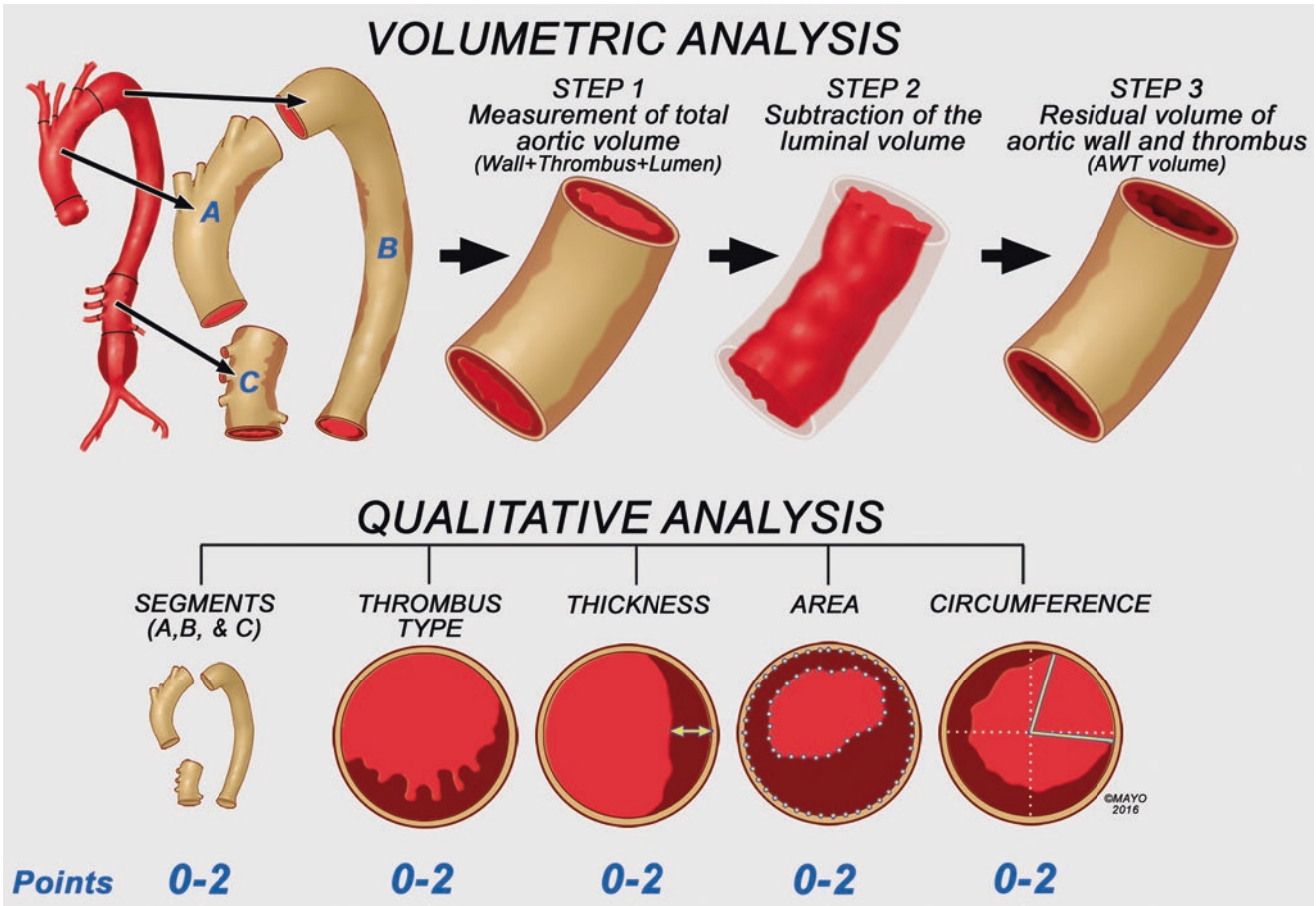

Fig. 11.38 Proposed Mayo Clinic grading system for assessment of aortic debris using volumetric and qualitative analysis using computed tomography angiography. By permission of Mayo Foundation for Medical Education and Research. All rights reserved

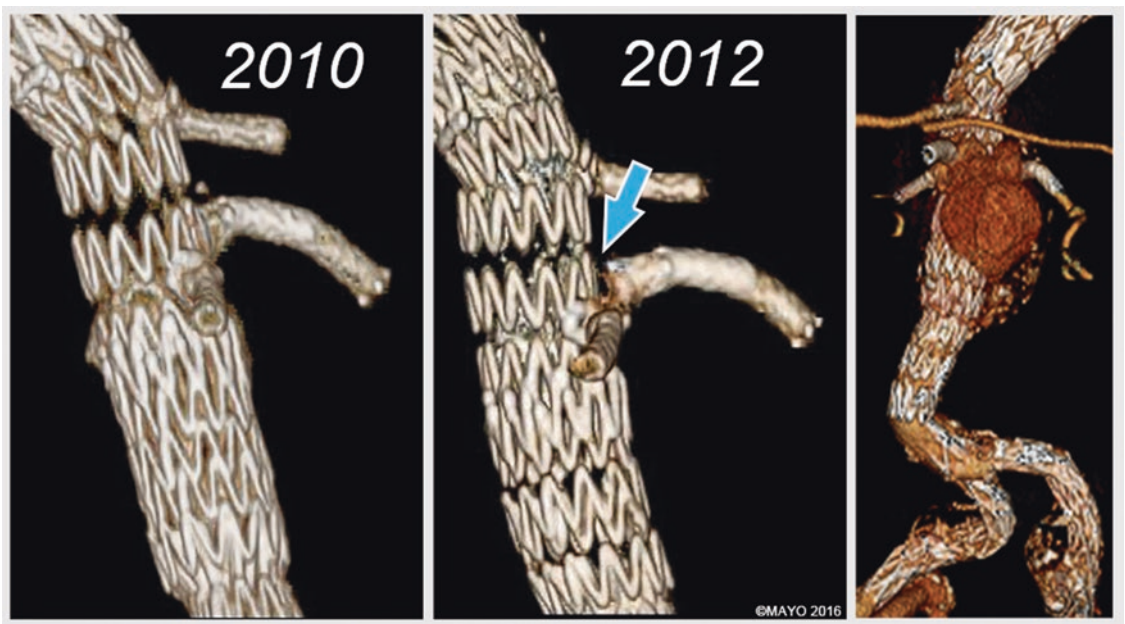

Fig. 11.39 Separation of components in a SMA fenestrated–branched stent caused a large Type IIIc endoleak, which was treated by redo stenting. By permission of Mayo Foundation for Medical Education and Research. All rights reserved

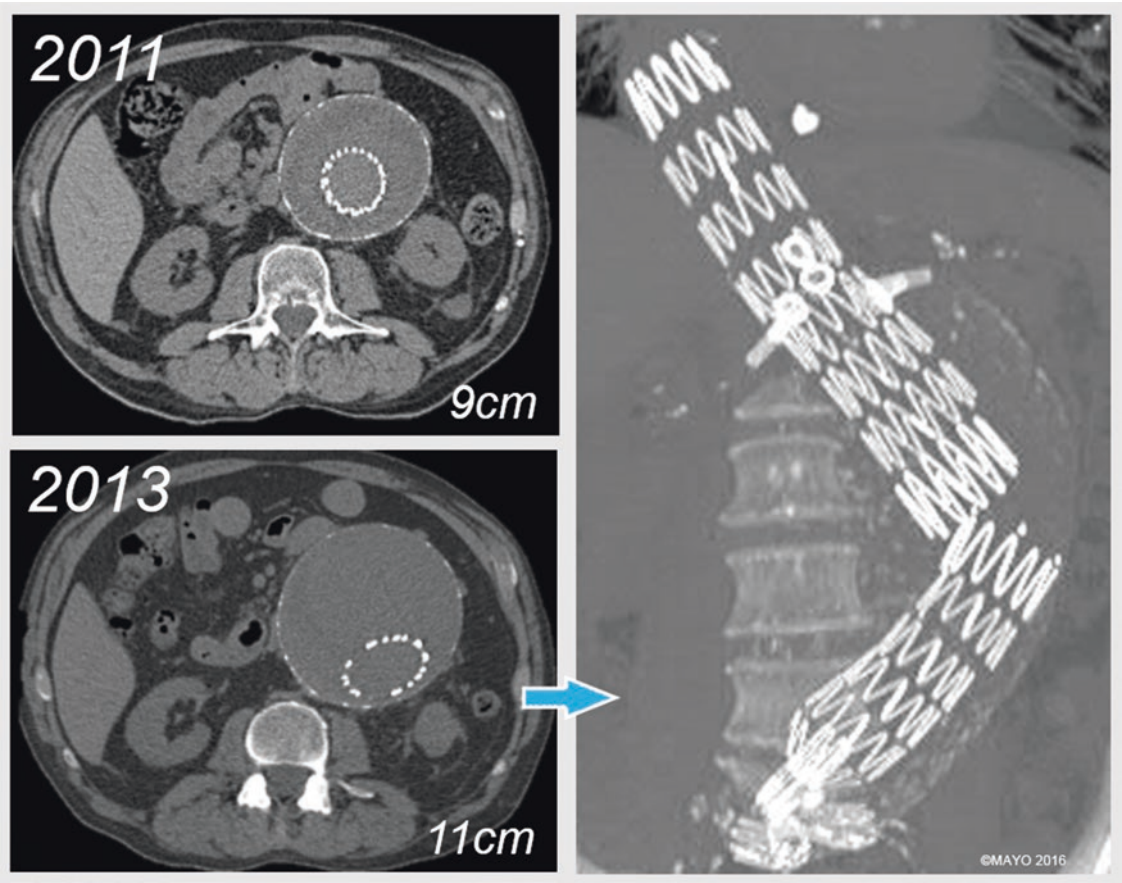

Fig. 11.40 Separation of distal bifurcated and proximal fenestrated components was treated by placement of tubular stent-graft. By permission of Mayo Foundation for Medical Education and Research. All rights reserved

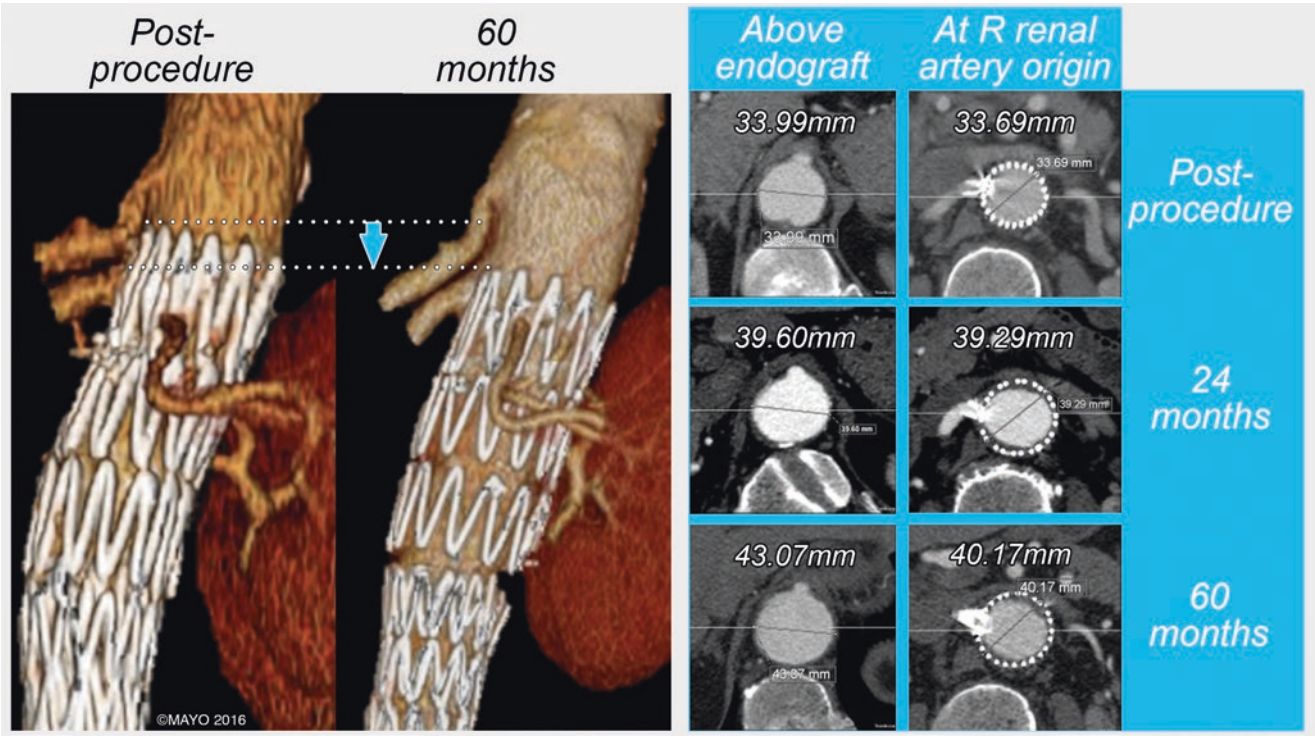

Fig. 11.41 Progression of aortic disease caused migration of the fenestrated stent-graft (*arrow*). By permission of Mayo Foundation for Medical Education and Research. All rights reserved

proper design, it can have devastating complications if not recognized. Progressive compression, dislodgement and loss of the renal stents can occur.

Device Integrity Issues

Device integrity failures are fortunately infrequent but can occur in the fabric (see Fig. 11.28) or metallic structure of the stent. These problems are manifested by endoleaks, complete graft disintegration, migration, and loss of seal zones.

Conclusion

CT angiography is an extremely powerful tool that provides a means to develop a detailed preoperative plan and detect any complications during follow-up before an issue manifests clinically. However, a clear understanding of the basics of CT scans and the methods of reconstruction and postprocessing techniques is required to accomplish these tests properly. Clinicians should be facile using postprocessing programs allowing the generation of MIPS, CLF reconstructions, and other tools that help define the vascular anatomy and pathology without an incision or an intervention.

Suggested Reading

1. Picel AC, Kansal N. Essentials of endovascular abdominal aortic aneurysm repair imaging: preprocedural assessment. AJR Am J Roentgenol. 2014;203(4):W347–57.
2. Picel AC, Kansal N. Essentials of endovascular abdominal aortic aneurysm repair imaging: postprocedure surveillance and complications. AJR Am J Roentgenol. 2014;203(4):W358–72.
3. Rossi M, Iezzi R. Cardiovascular and Interventional Radiological Society of Europe guidelines on endovascular treatment in aortoiliac arterial disease. Cardiovasc Intervent Radiol. 2014;37(1):13–25.
4. Wadgaonkar AD, Black III JH, Weihe EK, Zimmerman SL, Fishman EK, Johnson PT. Abdominal aortic aneurysms revisited: MDCT with multiplanar reconstructions for identifying indicators of instability in the pre- and postoperative patient. Radiographics. 2015;35(1):254–68.
5. Kalva SP, Dill KE, Bandyk DF, et al. ACR Appropriateness Criteria(R) nontraumatic aortic disease. J Thorac Imaging. 2014;29:W85–8.
6. Ambler GK, Coughlin PA, Hayes PD, Varty K, Gohel MS, Boyle JR. Incidence and outcomes of severe renal impairment following ruptured abdominal aortic aneurysm repair. Eur J Vasc Endovasc Surg. 2015;50(4):443–9.
7. Goldfarb S, McCullough PA, McDermott J, Gay SB. Contrast-induced acute kidney injury: specialty-specific protocols for interventional radiology, diagnostic computed tomography radiology, and interventional cardiology. Mayo Clin Proc. 2009;84:170–9.
8. McDonald RJ, McDonald JS, Carter RE, et al. Intravenous contrast material exposure is not an independent risk factor for dialysis or mortality. Radiology. 2014;273:714–25.
9. Yu L, Fletcher JG, Grant KL, Carter RE, Hough DM, Barlow JM, et al. Automatic selection of tube potential for radiation dose reduction in vascular and contrast-enhanced abdominopelvic CT. AJR Am J Roentgenol. 2013;201(2):W297–306.
10. McCollough CH, Primak AN, Braun N, Kofler J, Yu L, Christner J. Strategies for reducing radiation dose in CT. Radiol Clin North Am. 2009;47:27–40.
11. Yu L, Li H, Fletcher JG, McCollough CH. Automatic selection of tube potential for radiation dose reduction in CT: a general strategy. Med Phys. 2010;37:234–43.
12. Buls N, Van Gompel G, Van Cauteren T, et al. Contrast agent and radiation dose reduction in abdominal CT by a combination of low tube voltage and advanced image reconstruction algorithms. Eur Radiol. 2015;25:1023–31.
13. Winklehner A, Goetti R, Baumueller S, et al. Automated attenuation-based tube potential selection for thoracoabdominal computed tomography angiography: improved dose effectiveness. Invest Radiol. 2011;46:767–73.
14. Petersilka M, Bruder H, Krauss B, Stierstorfer K, Flohr TG. Technical principles of dual source CT. Eur J Radiol. 2008;68:362–8.
15. Megibow AJ, Sahani D. Best practice: implementation and use of abdominal dual-energy CT in routine patient care. AJR Am J Roentgenol. 2012;199:S71–7.
16. Sommer WH, Graser A, Becker CR, et al. Image quality of virtual non-contrast images derived from dual-energy CT angiography after endovascular aneurysm repair. J Vasc Interv Radiol. 2010;21(3):315–21.
17. Flors L, Leiva-Salinas C, Norton PT, Patrie JT, Hagspiel KD. Endoleak detection after endovascular repair of thoracic aortic aneurysm using dual-source dual-energy CT: suitable scanning protocols and potential radiation dose reduction. AJR Am J Roentgenol. 2013;200(2):451–60.
18. Chandarana H, Godoy MC, Vlahos I, et al. Abdominal aorta: evaluation with dual-source dual-energy multidetector CT after endovascular repair of aneurysms—initial observations. Radiology. 2008;249(2):692–700.
19. Stolzmann P, Frauenfelder T, Pfammatter T, et al. Endoleaks after endovascular abdominal aortic aneurysm repair: detection with dual-energy dual-source CT. Radiology. 2008;249(2):682–91.
20. Ascenti G, Mazziotti S, Lamberto S, et al. Dual-energy CT for detection of endoleaks after endovascular abdominal aneurysm repair: usefulness of colored iodine overlay. AJR Am J Roentgenol. 2011;196(6):1408–14.
21. Maturen KE, Kaza RK, Liu PS, Quint LE, Khalatbari SH, Platt JF. "Sweet spot" for endoleak detection: optimizing contrast to noise using low keV reconstructions from fast-switch kVp dual-energy CT. J Comput Assist Tomogr. 2012;36(1):83–7.
22. Albrecht MH, Scholtz JE, Husers K, et al. Advanced image-based virtual monoenergetic dual-energy CT angiography of the abdomen: optimization of kiloelectron volt settings to improve image contrast. Eur Radiol. 2016;26(6):1863–70.